Clays and Clay Minerals, Vol. 59, No. 3, 250–276, 2011.

MINERALOGICAL AND GEOCHEMICAL CHARACTERISTICS AND GENESIS OF HYDROTHERMAL KAOLINITE DEPOSITS WITHIN NEOGENE VOLCANITES, KÜTAHYA (WESTERN ANATOLIA), TURKEY

SELAHATTİN KADİR*, HANDE ERMAN, AND HÜLYA ERKOYUN

Eskişehir Osmangazi University, Department of Geological Engineering, TR-26480 Eskişehir, Turkey

Abstract—The Kütahya kaolinite deposits are the most important source of raw materials for the ceramics industry in Turkey. To date, no detailed mineralogical or geochemical characterizations of these materials have been carried out; the present study aims to fill that gap. The Kütahya kaolinite deposits formed by alteration of dacite and andesite tuffs related to Neogene volcanism which was associated with extensional tectonics. The kaolinite deposits contain silica and Fe- and Ti-bearing phases (pyrite, goethite, and rutile) in vertical and subvertical veins that diminish and then disappear upward. Mineralogical zonation outward from the main kaolinite deposit is as follows: kaolinite ± smectite + illite + opal-CT + feldspar; feldspar + kaolinite + quartz + smectite + illite; quartz + feldspar + volcanic glass. The veins and mineral distributions demonstrate that hydrothermal alteration was the main process in the development of the kaolinite deposits of the area. The very sharp, intense, diagnostic basal reflections at 7.2 and 3.57 Å, as well as non-basal reflections, well defined pseudohexagonal to hexagonal crystallinity with regular outlines, ideal differential thermal analysis-thermal gravimetric curves, and ideal, sharp, infrared spectral bands indicate well crystallized kaolinite. Micromorphologically, the development of kaolinite plates at the edges of altered feldspar and devitrified volcanic glass indicates an authigenic origin. Lateral increase in $(SiO_2+Fe_2O_3+MgO+Na_2O+CaO+K_2O)/(Al_2O_3+TiO_2)$ from the center of the kaolinite deposit outward also indicates hydrothermal zonation. Enrichment of Sr in altered and partially altered rocks relative to fresh volcanic-rock samples demonstrates retention of Sr and depletion of Rb, Ba, Ca, and K during hydrothermal alteration of sanidine and plagioclase within the volcanic units. In addition, depletion of heavy rare earth elements (*HREE*) relative to light rare earth elements (*LREE*) in the kaolinized materials may be attributed to the alteration of hornblende. The negative Eu anomaly suggests the alteration of feldspar by hydrothermal fluids. The isotopic data from kaolinite and smectite indicate that hydrothermal-alteration processes developed at 119.1−186.9ºC and 61.8−84.5ºC, respectively. Thus, the kaolinite deposits formed by hydrothermal alteration of volcanic glass, feldspar, and hornblende by a dissolution-precipitation mechanism which operated under acidic conditions within Neogene dacite, andesite, and tuffs.

Key Words—Geochemistry, Hydrothermal Alteration, Kütahya, Kaolinite, Mineralogy, Micromorphology, Neogene, Turkey, Volcanite.

INTRODUCTION

The Kütahya kaolinite deposits are the most important sources of raw material for the ceramic, tile, and paper industries in Turkey. These deposits have 1,350,000 tons of (inferred) minable reserves and 4,371,000 tons of inferred + probable reserves (8th Five-Year Development Plan – State Planning Organization of Turkey, 2001). Kaolinization and related alteration developed in Neogene volcanites as a result of hydrothermal activity. The geology (Okut *et al.*, 1978; Akdeniz and Konak, 1979a, 1979b; Özcan *et al.*, 1988; Üstün and Yetiş, 2007), mineralogy, and geochemistry (Şener and Gevrek, 1986; Ercan *et al.*, 1981−1982; 1978; Türkmenoğlu and Işık, 2008; Çoban, 2001; Işık *et al.*, 2001; Yıldız and Kuşçu, 2001; Sayın, 2007) of the area have been studied. Although Sayın (2007) studied the origin of the Hisarcık (Emet-Kütahya) kaolin deposits, no information concerning the general distribution of kaolinite deposits (besides the Hisarcık, Yüylük, Akçaalan, and Yağmurlar areas) of the Kütahya area is available, and no detailed mineralogical (polarized-light microscopy, infrared spectra), micromorphological (scanning and transmission electron microscopy), geochemical (modeling of mass gains and losses of major-, trace-, and rare-earth elements during alteration, and mineral chemistry), or kaolinite-fraction stable isotopic (including calculation of formation temperatures) studies of the kaolinite deposits of the area have been carried out. The main aim of the present study was to bridge this gap and to elucidate the mineralogy, micromorphology, geochemistry, and stable-isotope geochemistry of the Kütahya kaolinite ± halloysite and smectites within the host volcanites of the area to explain the hydrothermal-alteration processes suggested to have led to the formation of kaolinite in the Kütahya region. The

* E-mail address of corresponding author:
skadir_esogu@yahoo.com
DOI: 10.1346/CCMN.2011.0590304

paragenetic sequences and mineralogical distributions of the kaolinite deposits will be correlated on the basis of these data. The study provides new data and interpretations to guide future exploration of hydrothermal-alteration systems and related kaolinite deposits.

GEOLOGIC SETTING

The basement of the study area comprises Precambrian gneiss and migmatite, known as the Kalkan Formation (Figures 1, 2), which is overlain by the Paleozoic Menderes Massif metamorphics, comprising mica schist, quartzite, and garnet schist (Okut *et al.*, 1978). The Menderes Massif metamorphics are overlain by recrystallized limestones. Carbonate units and ophiolitic mélange make up Mesozoic units. A late-Cretaceous ophiolitic mélange consists of various ultrabasic rocks overlain by calcareous units, recrystallized limestone, and schist. The ophiolitic mélange is cross-cut by the Paleocene Eğrigöz granitoid. Lower Miocene volcano-sedimentary rocks are made up of conglomerates and sandstones within cataclastic facies, marl, clayey limestones (with gastropods), and volcanic tuff-tuffite, which in turn are overlain by Neogene lacustrine sediments. Rhyolitic, rhyodacitic, and dacitic lavas and tuffs were laid down in the Middle Miocene (the Civanadağ tuffs), and Upper Miocene trachyandesite, andesite, andesitic basalt, and pyroclastic rocks make up the Akdağ volcanites (Helvacı, 1984; Seyitoğlu *et al.*, 1997). Above these are Pliocene lacustrine sediments and these volcanic units are in turn overlain by undifferentiated Quaternary continental clastic rocks, lacustrine limestone, and travertine. In the study area, rhyolitic, rhyodacitic, dacitic, and andesitic rocks are kaolinized. Geochronological results from the Aegean islands and western Anatolia indicate that calc-alkaline volcanism developed in the Middle Miocene and continued during the Late Miocene and Pliocene (Ercan *et al.*, 1978). Based on stratigraphic and paleontological data, the volcanic activity took place during the Pliocene (Okut *et al.*, 1978). NW–SE-oriented grabens (*e.g.* Kütahya graben, Simav graben) developed in the Menderes Massif (Aegean region) during the Miocene, and alkaline volcanic activity was related to normal faults (Ercan *et al.*, 1981–1982; Çiftçi and Bozkurt, 2009). The

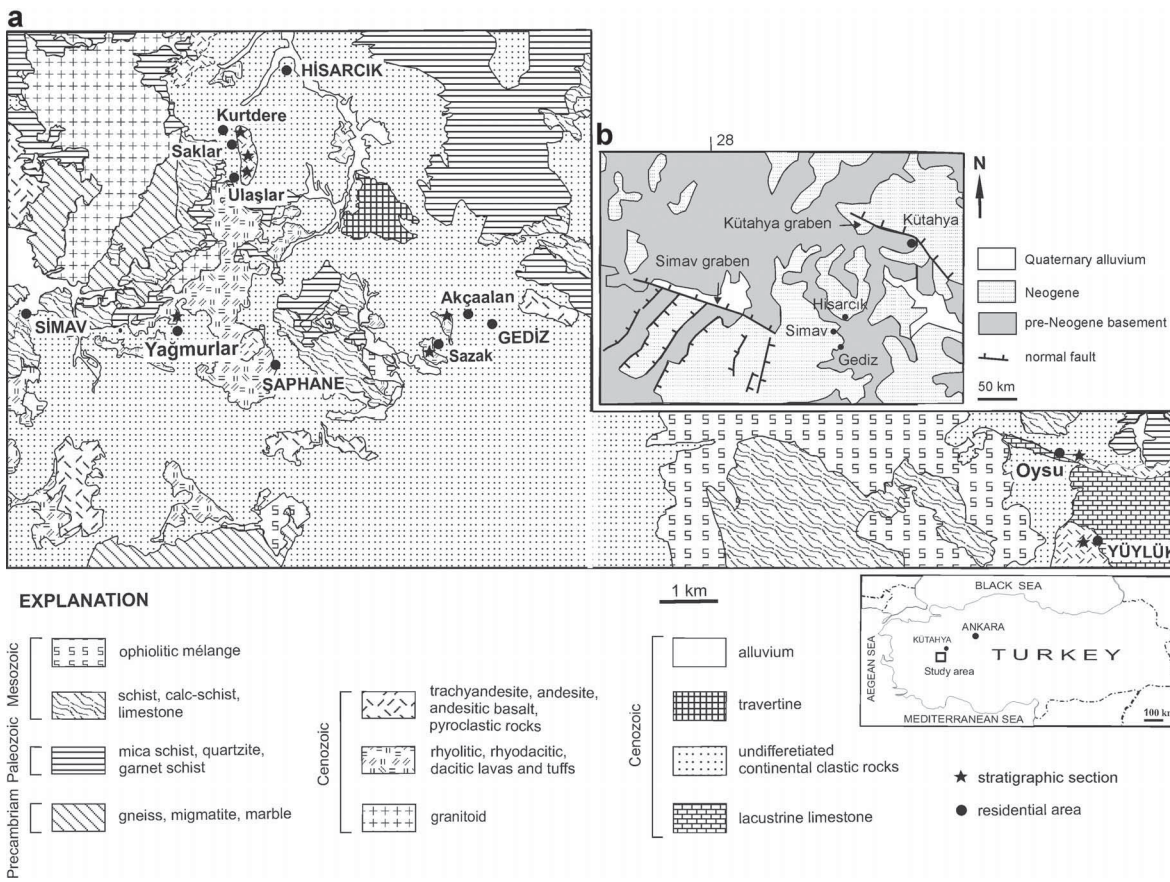

Figure 1. Geologic (a) and tectonic (b) maps of the Kütahya kaolinite deposit and surrounding area (modified from Konak, 2007; Çiftçi and Bozkurt, 2009).

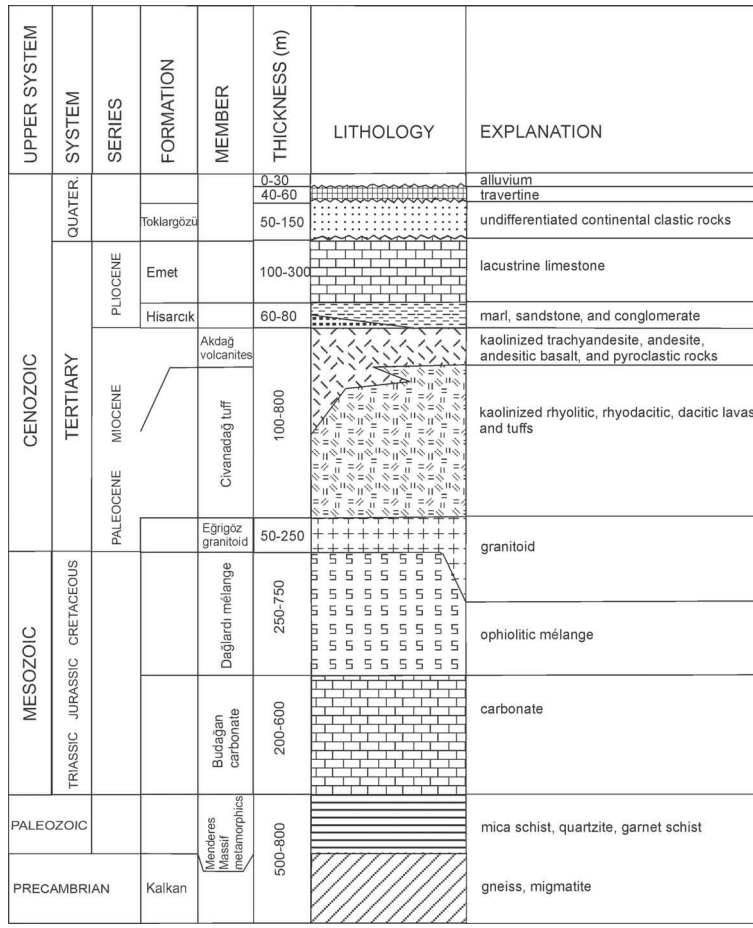

Figure 2. Simplified general stratigraphic section for the study area (modified from Akdeniz and Konak, 1979b).

resulting volcanic rocks may have been derived from the paleosubduction zone that developed as a result of collision of the African and Aegean platforms in the Early Miocene (Savaşçın, 1978). K-Ar studies have revealed the age of volcanic rocks around the Şaphane area (Kütahya) to be 12–13 Ma (Middle Miocene) (Mutlu *et al*., 2005).

GENERAL FEATURES OF THE KAOLINITE DEPOSITS

Yüylük area

Dacite, andesite, and tuff exposed south of the Yüylük area are kaolinized (Figures 1, 3). The volcanic units are grayish-white overall, have weak Fe (oxyhydr)-oxide staining, are silicified, and the feldspar is kaolinized. Silicification, brecciation, and Fe (oxyhydr)-oxide veins occur in the lower levels of these units. A pale gray-white to yellow kaolinized zone contains subvertical yellowish to reddish Fe (oxyhydr)oxide-bearing veins, 20–30 cm thick, which thin upward, with capillary silicic veins in the lower part of the kaolinized zone. The kaolinized zone is 10 m thick and 9 m wide. A dark brownish-red, hard, conchoidally fractured, silicified zone occurs in the uppermost part of the deposit.

Hisarcık area

The Hisarcık area hosts three kaolinite deposits, namely, the Kurtdere, Ulaşlar, and Saklar deposits (Figures 1, 3). Volcanic units of the Hisarcık area consist of dacite, rhyodacite, trachyandesite, and tuffs having gradational contacts with white to yellowish-white, moderately hard kaolinized and silicified zones. The kaolinite is multicolored, soft to moderately hard, and friable, and contains Fe (oxyhydr)oxide veins. A yellowish-brown, Fe (oxyhydr)oxide stockwork-type zone, 5–30 cm thick, occurs between the kaolinite and silicified zones. The kaolinite deposit is covered by a hard silica cap zone, 1 m thick, which is between the kaolinite zone and volcanic materials. These veins have a brecciated character in the Ulaşlar kaolinite deposit, cross-cutting volcanic material. This zone is also cross-cut by secondary calcite veins 5–10 mm thick.

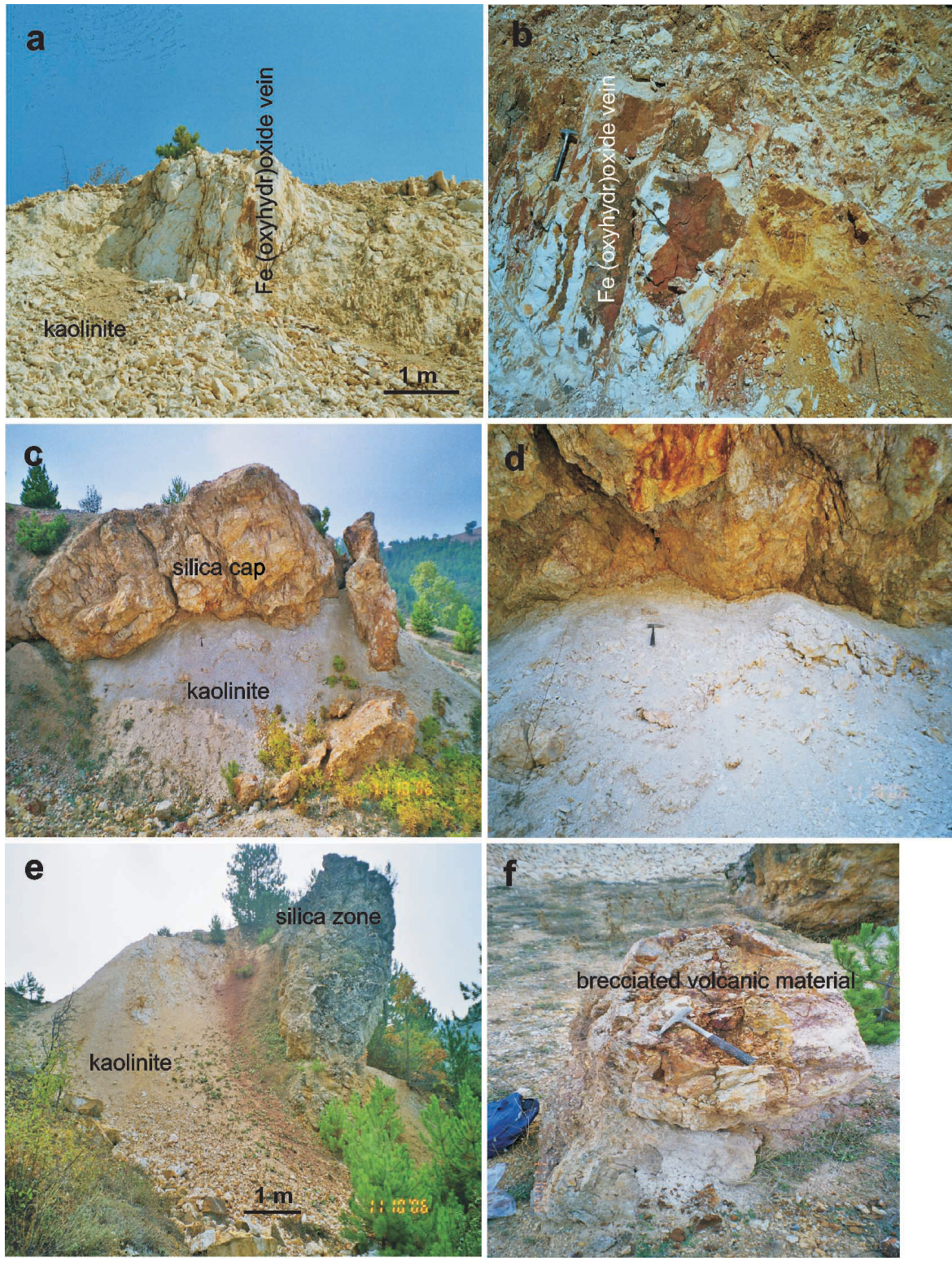

Figure 3. (a) Fe (oxyhydr)oxide-bearing phases, along subvertical fractures in the Ulaşlar kaolinite deposit; (b) close-up view of Fe (oxyhydr)oxide-bearing phases in kaolinized units of the Yüylük kaolinite deposit; (c–d) silica cap on the Ulaşlar kaolinite deposit; (e) close relationship between a subvertical silica zone and kaolinized volcanic material in the Kurtdere kaolinite deposit; (f) close-up view of Fe (oxyhydr)oxide-cemented brecciated volcanic material in the Ulaşlar kaolinite deposit.

Simav area

The Yağmurlar deposit is the main kaolinite deposit in the Simav area. Dacite, andesite, and tuff and, in particular, vitric tuff are the main host rocks of the kaolinite deposit. The kaolinite is white to yellow, soft to moderately hard, friable, and contains Fe (oxyhydr)-oxide concentrations that fill dissolution voids and fractures, and also bears relicts of gray, partially altered tuffaceous materials. The kaolinite deposit is ~300 m long and ~25 m thick. A brownish-red, hard, conchoidally fractured silicified zone, ~3 m thick, occurs in the uppermost part of the deposit.

Gediz area

The kaolinite deposits of the Gediz district occur in the Akçaalan and Sazak areas. Kaolinization occurs within a Neogene lacustrine facies and volcanic rocks consisting of andesite, rhyodacite, and tuffs. Green and variably dark-colored tuff is massive and hard, with angular fracture, in volcanic units of the Akçaalan area. Kaolinite is grayish-white to beige, moderately hard, and laminated, coated by Fe (oxyhydr)oxide. A silica cap is dark gray, blocky, and consists of silicified rhyodacite, dacite, trachyandesite, andesite, and tuffs in the upper part of the deposit.

METHODS

In order to identify the lateral and vertical distribution of kaolinite and coexisting clay and non-clay minerals in the study areas, the kaolinite deposits were sampled (Figures 1, 2). One hundred and thirty samples, representing various degrees of alteration, were analyzed using polarized-light microscopy (Leitz Laborlux 11 Pol), powder X-ray diffractometry (XRD) (Rigaku-Geigerflex), scanning electron microscopy (SEM-EDX) (JEOL JSM 84A-EDX), transmission electron microscopy (TEM) (JEOL JEM-21007), differential thermal analysis-thermal gravimetry (DTA-TG) (Rigaku TAS 100 E), and Fourier-transform infrared (FTIR) spectroscopy (PerkinElmer 100 FTIR spectrometer) in order to determine their mineralogical characteristics. The XRD analyses were performed using CuKα radiation and a scanning speed of 1º2θ/min. The samples were ground using an agate mortar and pestle. Randomly oriented powders from whole-rock samples were used to determine the bulk mineralogy. The samples were treated chemically in 1 N acetic acid, boiled for 2.5 min with 0.5 N NaOH solution, and subjected to the sodium dithionite-citrate method (Kunze and Dixon, 1986) to remove carbonates, amorphous silica, and free Fe oxides. After each chemical treatment, the samples were washed with distilled water. The clay mineralogy was determined by separation of the <2 μm fraction by sedimentation according to Stokes Law, followed by centrifugation of the suspension using a speed of 5000 rpm/10 min, after overnight dispersion in distilled water. The clay particles were dispersed by ultrasonic vibration for ~15 min. Four oriented specimens of the <2 μm fraction were prepared from each sample, air-dried, ethylene glycol-solvated at 60ºC for 2 h, and thermally treated at 350ºC and 550ºC for 2 h. Semi-quantitative relative abundances of rock-forming minerals were obtained according to the method of Brindley (1980), whereas the relative abundances of clay-mineral fractions were determined using their basal reflections and the intensity factors of Moore and Reynolds (1989). The presence of Fe (oxyhydr)oxide was determined by reflected-light microscopy (Leitz MPV-SP). Representative clay-rich bulk samples were prepared for SEM-EDX analysis by adhering the fresh, broken surface of each rock sample onto an aluminum sample holder using double-sided tape, and then coated with a thin film (~ 350 Å) of gold using a Giko ion coater.

The clay particles for TEM analysis were dispersed in an ultrasonic ethanol bath for ~30 min, and one drop of clay suspension was placed on a carbon-coated copper grid and dried at room temperature. The DTA-TG curves were obtained using 10 mg of powdered clay sample in a Pt sample holder at an average heating rate of 10ºC min^{-1} with an alumina reference. The FTIR spectroscopic analysis was performed on pressed pellets of powdered clay samples (2 mg of <2 μm fraction) mixed with 200 mg of KBr; scans were made at 4 cm^{-1} resolution.

Chemical analyses of 42 whole-rock samples and three purified kaolinite and one purified smectite samples were carried out using inductively coupled plasma atomic emission spectroscopy (ICP-AES) for major and trace elements at Acme Analytical Laboratories, Ltd. (Canada). The detection limits for the analyses were between 0.01 and 0.1 wt.% for major elements, and between 0.1 and 5 ppm for trace elements.

Enrichments and depletions of elements were estimated using the procedure of MacLean and Kranidiotis (1987). In these calculations, Zr was assumed to be the most immobile element based upon calculated correlation coefficients with other elements. All samples were grouped on the basis of degree of alteration (average result from each group), and the gains and losses of components were calculated using a starting mass of 100 g of average, fresh, anhydrous sample. The equation used in the calculations can be written for SiO_2 (MacLean and Kranidiotis, 1987) as:

$$SiO_2 = \frac{SiO_2 \text{ wt.\% altered rock}}{\text{Zr ppm altered rock}} \times \text{Zr ppm fresh rock}$$

Gains and losses of mass (ΔC_i) for each element were determined by subtracting the calculated values (RC) from the concentrations of components in the least-altered samples using the formula above.

Structural formulae for kaolinite and smectite were determined on <2 μm clay-fraction samples, with the largest kaolinite and smectite contents prepared by

separation of the clay fraction by sedimentation, followed by centrifugation of the suspension after overnight dispersion in distilled water. The structural formulae of kaolinite were calculated based on $O_{10}(OH)_8$, and of smectite based on $O_{20}(OH)_4$ using the following assumptions: the tetrahedral sites of kaolinite were filled with Si and Al to sum to four, and tetrahedral sites of smectite were filled with Si and Al to sum to eight. The remaining Al was assigned to octahedral sites. All Fe was assumed to be ferric, and all Mn and Ti were assigned to the octahedral site. Ca, Na, K, and P were deemed to be exchangeable interlayer cations. Phosphorus can be also adsorbed on the surfaces of kaolinite and smectite crystals (Pissaridges *et al*., 1968).

Five kaolinite- and three smectite-bearing samples were purified and analyzed for the stable isotopes of H and O by Activation Laboratories, Ltd. (Actlabs), Canada. The H-isotopic analyses, by conventional isotope-ratio mass spectrometry, are reported in familiar notation, per mil (‰) relative to the V-SMOW standard. The procedure described above was used to measure a δD value of −65‰ for the NSB-30 biotite standard. The O-isotopic analyses were performed using a Finnigan MAT Delta, dual inlet, isotope-ratio mass spectrometer, following the procedures of Clayton and Mayeda (1963). The data are reported in the standard delta notation as per mil deviations from V-SMOW. External reproducibility was ±0.19‰ (1σ) based on repeat analyses of an internal white crystal standard (WCS). The NBS 28 value is 9.61±0.10‰ (1σ).

RESULTS

Petrography

The volcanic units of the Kütahya kaolinite district consist of dacite, andesite, and tuff (Figure 4). The units are mainly porphyritic, and the phenocrysts are typically composed of twinned and locally zoned plagioclase (andesine-labradorite), cloudy carlsbad-twinned sanidine, hornblende, biotite, opaque minerals, and accessory garnet, all cemented by volcanic glass and microlitic plagioclase-type groundmass (Figure 4a–d). Varying degrees of alteration were determined in these units. Generally, plagioclase phenocrysts showed degradation and argillization, hornblende and biotite have been re-opacitized and chloritized, sanidine has been sericitized and argillized, and quartz has been extremely fragmented and cemented by micronetworks of pale brown-yellowish, locally reddish-brown, Fe (oxyhydr)-oxide (Figure 4c–e).

Tuffaceous units generally consist of relatively scarce plagioclase, hornblende, opaque minerals, rock fragments, glass shards, quartz, and, locally, chalcedony, cemented by amorphous glassy volcanic groundmass (characteristic of the vitric and lithic tuffs) (Figure 4f–h).

Stockwork-type fractures and fissures in the groundmass and enclosed phenocrysts are filled by Fe (oxyhydr)oxide, opacitized materials, and silica (Figure 4e–g). Sieve textures, Fe oxidation, and blackish and yellowish 'spongy' alteration are visible in plane-polarized light (Figure 4h). Carbonate cement and argillized groundmass occur locally. Volcanic glass shards are devitrified and coexist with irregular, blackish-brown Fe (oxyhydr)oxide phases; locally, spherulitic texture – replaced by a chalcedony-like mineral – is present. Thus, alteration types in the Kütahya volcanic units are generally kaolinization, sericitization, Fe (oxyhydr)oxidation, chloritization, and silicification, as well as weak zeolitization locally.

Pyrite, goethite/lepidocrocite, and hematite were determined using reflected-light microscopy. Pyrite was transformed locally to hematite.

Clay mineralogy

The mineral assemblages obtained by XRD for bulk samples from the Yüylük, Ulaşlar, Saklar, Kurtdere, Yağmurlar, Akçaalan, and Sazak kaolinite deposits (Table 1) reveal that kaolinite is the predominant clay mineral and is generally associated with accessory smectite ± illite. Smectite is also locally abundant. The clay minerals are accompanied by feldspar, quartz, and opal-CT and, locally, alunite, pyrite, aragonite, calcite, dolomite, and amphibole. Opal-CT predominates, but quartz is abundant in some of the samples. An inverse relationship exists between feldspar and clay minerals.

The kaolinite was identified by narrow, sharp peaks at 7.20 and 3.57 Å, with less intense, non-basal reflections consisting of triplets and doublets at 4.48, 4.37, 4.17; 2.56, 2.50; and 2.39, 2.34, and 2.30 Å, indicating well crystallized kaolinite (Brindley, 1980; Wilson, 1987) (Figure 5). The basal reflection at 7.20 Å was reduced at 350ºC and collapsed at 550ºC due to dehydroxylation. Smectite was identified by a peak at 15.34 Å (Figure 5). This peak expanded to 17.20 Å following ethylene glycol solvation, and collapsed to 9.90 Å upon heating to 350ºC; additional heating to 550ºC caused further reduction in sharpness and reflection of the peaks. The d_{060} reflection may indicate the occurrence of dioctahedral smectite (Moore and Reynolds, 1989). Illite was indicated by reflections at 10 and 5 Å.

SEM-EDX determinations

Scanning electron microscopy determinations revealed that kaolinite ± halloysite and smectite-illite were the main alteration products of volcanic glass and feldspar in the volcanic units (Figure 6). Kaolinite occurs either as degraded plates in dissolution voids and fractures – possibly due to flushing of hydrothermal fluids – or as euhedral pseudohexagonal and hexagonal crystals, exhibiting book-like kaolinite locally at the edges of altered feldspars and glass shards (Figure 6a–d). Kaolinite

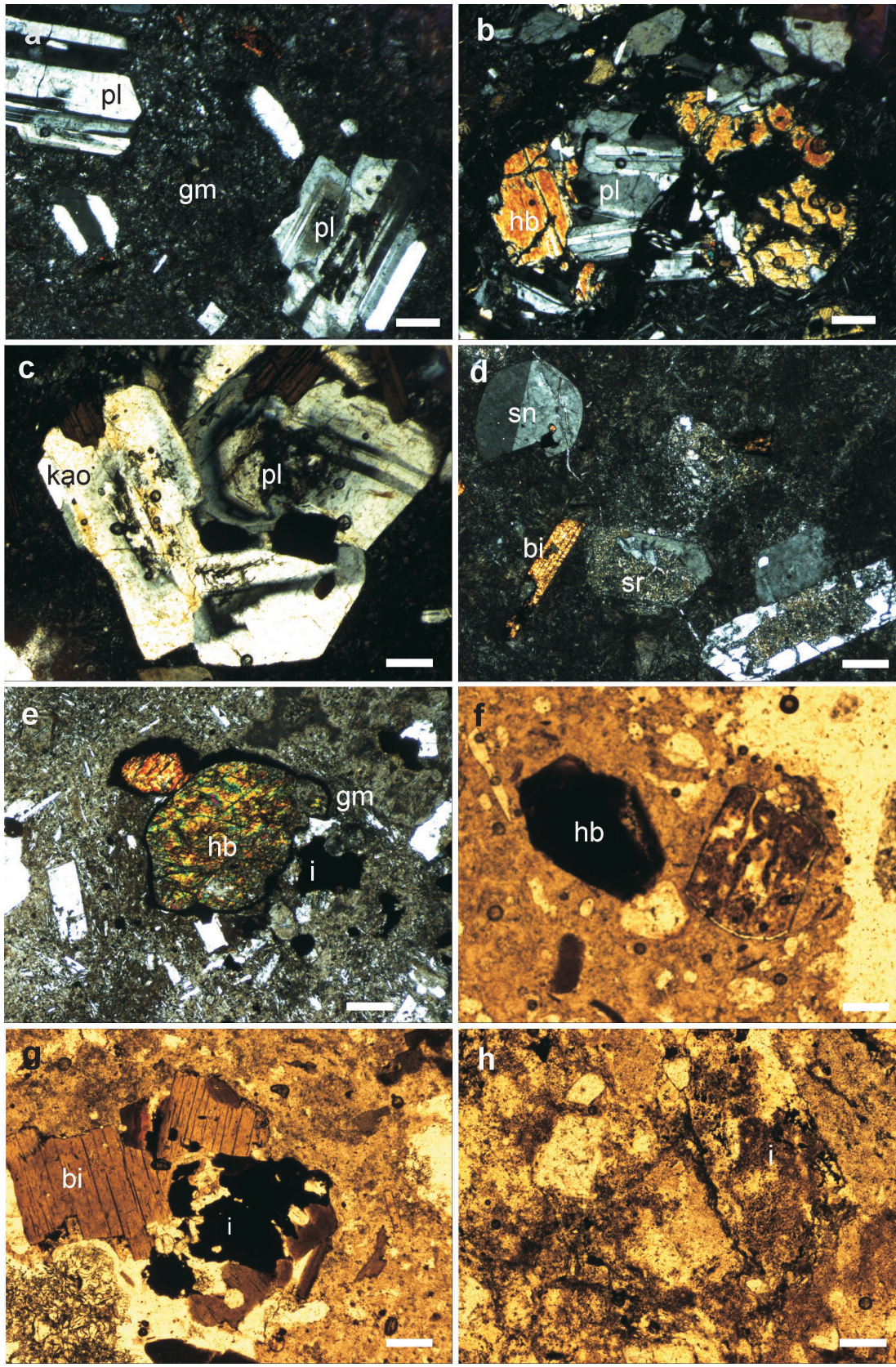
a
pl
gm
pl
b
pl
hb
c
kao
pl
d
sn
bi
sr
e
gm
hb
i
f
hb
g
bi
i
h
i

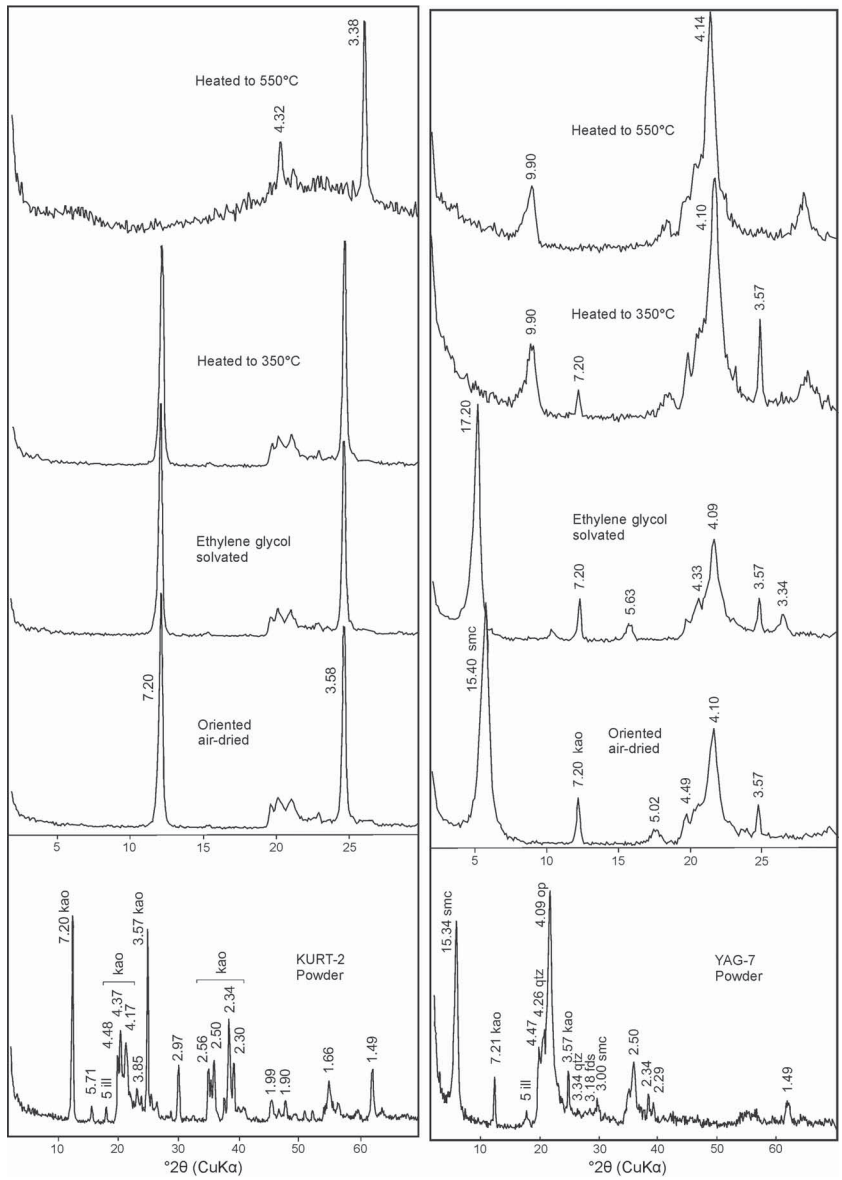

Figure 5. XRD patterns of kaolinite-rich (KURT-2) and smectite-rich (YAG-7) samples. kao – kaolinite; smc – smectite; ill – illite; qtz – quartz; op – opal-CT; fds – K-feldspar.

crystals are 2 to 5 μm wide. Halloysite occurs as fibers, fiber meshes, and thin rods (2–4 μm long) edging blocky, altered feldspar crystals in volcanic units (Figure 6e–h). Rod-like halloysite covers kaolinite plates in sample SAK-5, suggesting a genetic relationship (Figure 6h). Smectite with cornflake-like textures occurs as pore bridges developed in finer-grained smectite-dominated, altered volcanic material (Figure 6i, j). Illite occurs as fibers at the edges of smectite plates. Alteration products such as smectite and smectite-illite coexist with spherical forms (5–10 μm) consisting of accumulations of lepispheres or acicular crystals of opal-CT (Figure 6k,l). Halloysite was not detected by XRD, probably due to the low concentrations of that mineral.

Figure 4 (*facing page*). Photomicrographs: (a–b) degraded plagioclase and hornblende phenocrysts in a glassy groundmass; crossed nicols (AK-12, AK-8); (c) kaolinization of zoned plagioclase; crossed nicols (AK-12); (d) sericitization of sanidine; crossed nicols (S-1); (e) Fe-oxidized hornblende in a plagioclase-microlite-rich groundmass; crossed nicols (AK-13); (f) opacitized hornblende; plane-polarized light (UL-16); (g) opacitized biotite in Fe-oxidized, altered tuff; plane-polarized light (UL-18); (h) Fe-oxidized crystal tuff; plane-polarized light (YAG-25). Index: pl – plagioclase, gm – groundmass, hb – hornblende, sn – sanidine, bi – biotite, kao – kaolinite, sr – sericite, i – Fe (oxyhydr)oxide. Scale bar = 0.1 mm.

Table 1. Mineralogical variation within the Kütahya kaolinite deposits and surrounding area. kao – kaolinite, smc – smectite, ill – illite, gyp/anh – gypsum/anhydrite, fds – feldspar, qtz – quartz, op – opal-CT, arg – aragonite, cal – calcite, dol – dolomite, amp – amphibole. Acc – accessory, + – relative abundance of mineral.

Sample	Rock type	kao	smc	ill	gyp/anh	fds	qtz	op	arg	cal	dol	amp
YUY-2	Silicified tuff	++	Acc				+++					
YUY-4	Silicified tuff	+				Acc	+	++++				
YUY-5	Silicified tuff	+				Acc	+	++++				
YUY-7	Silicified tuff						+++++					
YUY-8	Altered tuff	++	++	Acc		Acc	+	+		Acc		
YUY-10	Altered tuff	++++	Acc	Acc		Acc	+	Acc				
YUY-11	Partially altered tuff	+		Acc			+	++				
YUY-16	Altered tuff	++++	Acc	Acc			+	+				
YUY-17	Altered tuff	++++	Acc	Acc			+	+				
YUY-18	Altered tuff	+	+	+		Acc	+			++	+	Acc
YUY-19	Altered tuff	++++						+	Acc			
YUY-20	Altered tuff	++++	+	Acc			+	+				
YUY-21	Altered tuff	+++		Acc		Acc	+	++				
YUY-22	Altered tuff	+	Acc	Acc		Acc	+	+				
YUY-23	Altered tuff	+	Acc	Acc		Acc	+	++				
YUY-24	Altered tuff	++				Acc	+	++				
YUY-28	Silicified tuff	+	Acc		Acc	Acc	Acc	+++				
YUY-29	Silicified tuff	+		Acc		Acc	Acc	+++				
UL-1	Silicified tuff						+++++					
UL-2	Altered tuff	+				Acc	+	+++				
UL-3	Altered tuff	++	Acc	Acc		Acc	+	++				
UL-4	Silicified tuff						+++++					
UL-5	Altered tuff	++	+	Acc			+	++				
UL-6	Altered tuff	+++	+	Acc		Acc	Acc	++				
UL-8	Altered tuff	++	+	Acc		Acc	Acc	++				
UL-9	Altered tuff		+++	+		+	+	+				
UL-11	Altered tuff	+++					++					
UL-15	Silicified tuff	Acc	Acc				Acc			++++	Acc	
SAK-1	Altered tuff	++				Acc	Acc	+++				
SAK-2	Altered tuff	++					+	+				
SAK-4	Altered tuff	++	Acc			Acc	+	++				
SAK-5	Altered tuff	+++					+	++				
SAK-10	Altered tuff	++	+	Acc		Acc	Acc	+		Acc		Acc
SAK-16	Altered tuff	+	++	++		+	+					Acc
SAK-17	Altered tuff	+	Acc	Acc			Acc	+++				
SAK-19	Altered tuff	++	+	Acc		Acc	Acc	+++		Acc		Acc
SAK-20	Altered tuff	+++	Acc	Acc		Acc	Acc	++				
SAK-23	Altered tuff	+++	Acc	Acc		Acc	Acc	++				
SAK-24	Altered tuff	+	+++	+		Acc	+	Acc				Acc
SAK-25	Altered tuff	Acc	++	++		+	+			Acc		Acc
KURT-1	Partially altered tuff	Acc	Acc	Acc		Acc	+++			+		Acc
KURT-2	Altered tuff	++++						+				
KURT-3	Altered tuff	++	Acc				+	+				
KURT-5	Altered tuff	+++	Acc				+	+				
YAG-1	Altered tuff	+	++	Acc		Acc	Acc	+				
YAG-2	Altered tuff	+	+++	Acc		Acc	Acc	++				
YAG-4	Altered tuff	++	++	Acc				++				
YAG-5	Altered tuff	+	++	Acc		Acc	Acc	++				Acc
YAG-6	Altered tuff	Acc	++++	Acc		Acc	Acc	+				
YAG-7	Altered tuff	+	+++	Acc				++				
YAG-10	Altered tuff	++	+	Acc				++				
YAG-11	Altered tuff	+	+++			Acc	Acc	+				
YAG-12	Altered tuff	++	+	Acc		Acc	Acc	++				
YAG-15	Partially altered tuff	++	Acc			Acc	Acc	++				
YAG-16	Partially altered tuff	++					Acc	+++				
YAG-17	Altered tuff	++	Acc			Acc	Acc	+++				
YAG-19	Partially altered tuff	++					Acc	+++				
YAG-23	Altered tuff	Acc	Acc	+		+++		+				

Table 1 (*contd*.)

Sample	Rock type	kao	smc	ill	gyp/anh	fds	qtz	op	arg	cal	dol	amp
AK-4	Partially altered tuff		+	+		++	+	+				
AK-6	Partially altered tuff		++	Acc		++	Acc	Acc		Acc		
AK-9	Altered tuff	+	+			++		+		Acc		
AK-10	Altered tuff	++	++	Acc		++		Acc				
AK-14	Altered tuff	+	+	+		++	+	+		+		Acc
AK-17	Altered tuff	+	+	+		+		+				
S-2	Partially altered tuff	+	+			Acc		+++				Acc
S-3	Partially altered tuff	Acc	++	Acc		+	++					Acc
S-6	Partially altered tuff	+	Acc	Acc		+		++				
S-7	Altered tuff	++				+	Acc	++				
S-8	Altered tuff	Acc	+++	Acc		+	+	+		Acc		
S-9	Altered tuff	+	Acc	Acc		+		++				
S-10	Partially altered tuff	Acc	Acc	++		++		Acc			+	
S-14	Partially altered tuff	+		Acc		Acc	Acc	++		+	Acc	

Energy-dispersive X-ray (EDX) analysis of fiber meshes and thin rods of halloysite yielded nearly equally high peaks for Si and Al. The EDX analysis of fibrous illite crystals found at the edges of smectite revealed the elements Si, Al, and K.

Determinations by TEM revealed that kaolinite occurs in well defined pseudohexagonal to hexagonal crystals with regular outlines (Figure 7a–c). The diameters of kaolinite particles varied between 0.5 and 1.7 μm.

DTA-TG analyses

The reaction of Kütahya kaolinite samples to DTA-TG heating (Figure 8) yielded in sample UL-11 a symmetrical endothermic peak between 500 and 600ºC (weight loss: 13.49%), and a sharp exothermic peak at 1008ºC (weight loss: 1.0%). The peaks are attributed to the dehydroxylation of well crystallized kaolinite (MacKenzie, 1957; Paterson and Swaffield, 1987). The DTA-TG curves for sample UL-11 represent ideal, well crystallized kaolinite with typical thermal reactions (MacKenzie, 1957; Paterson and Swaffield, 1987).

The reaction of Kütahya smectite-dominated sample YAG-6 to heating yielded endothermic peaks at 35–280ºC (weight loss: 6.40%), 280–750ºC (weight loss: 5.88%), and 750–1100ºC (weight loss: 0.23%) (Figure 8). The first endothermic peak is due to the elimination of hygroscopic and zeolitic waters; the second endothermic peak is due to dehydroxylation (MacKenzie, 1957; Felhi *et al.*, 2008). The last endothermic peak is followed by an exothermic peak due to recrystallization into a possible enstatite phase (MacKenzie, 1957).

Infrared spectra

The FTIR spectra of a representative kaolinite sample, UL-11, (Figure 9) are characterized by sharp bands at 3686 and 3620 cm^{-1} and a weak band at 3651 cm^{-1}, all related to the inner OH-streching band of well crystallized kaolinite rather than dickite and nacrite, both of which have higher-frequency bands, as reported by Johnston *et al.* (1990), Benco *et al.* (2001), and Balan *et al.* (2001, 2005). The strong bands at 1115, 1026, 1004, 682, and 462 cm^{-1} are attributed to the Si–O stretching vibration (Farmer, 1974; Johnston *et al.*, 1990). The absorption band at 912 cm^{-1} reflects Al–OH, and that at 789 cm^{-1} corresponds to Fe–OH–Mg (Madejová *et al.*, 2002). The bands at 750 cm^{-1} are related to Al–OH deformation (Njoya *et al.*, 2006). The bands at 529 and 428 cm^{-1} are assigned to Si–O–Si (Al) (Bobos *et al.*, 2001).

The FTIR spectra for smectite-dominated sample YAG-6 revealed bands at 3696, 3624, 1637, 1118, 1006, 909, 793, 750, 685, 522, and 458 cm^{-1}, suggesting the presence of montmorillonite (Van der Marel and Beutelspacher, 1976) (Figure 9). The narrow band at 1637 cm^{-1} corresponds to the vibration of adsorbed water. The band at 793 cm^{-1} corresponds to Fe–OH–Mg. The bands at 522 and 458 cm^{-1} are assigned to Si–O–Si (Al) deformation. The OH and Si–O stretching bands are consistent with results from XRD, SEM, DTA-TG, and chemical analyses of the samples.

Geochemistry

Chemical analyses (Table 2) of whole rocks of samples of the volcanic host rocks (and their alteration products) of the Yüylük, Hisarcık, Simav, and Gediz areas revealed that fresh volcanic rocks and altered rocks plot in the rhyodacite, dacite, trachyandesite, and andesite fields in the Zr/TiO_2 *vs*. Nb/Y diagram (Winchester and Floyd, 1977) (Figure 10).

Using mass gains and losses (MacLean and Kranidiotis, 1987) of kaolinite samples from deposits in the Yüylük, Hisarcık, Simav, and Gediz areas, major- and trace-element variability appears to be related to

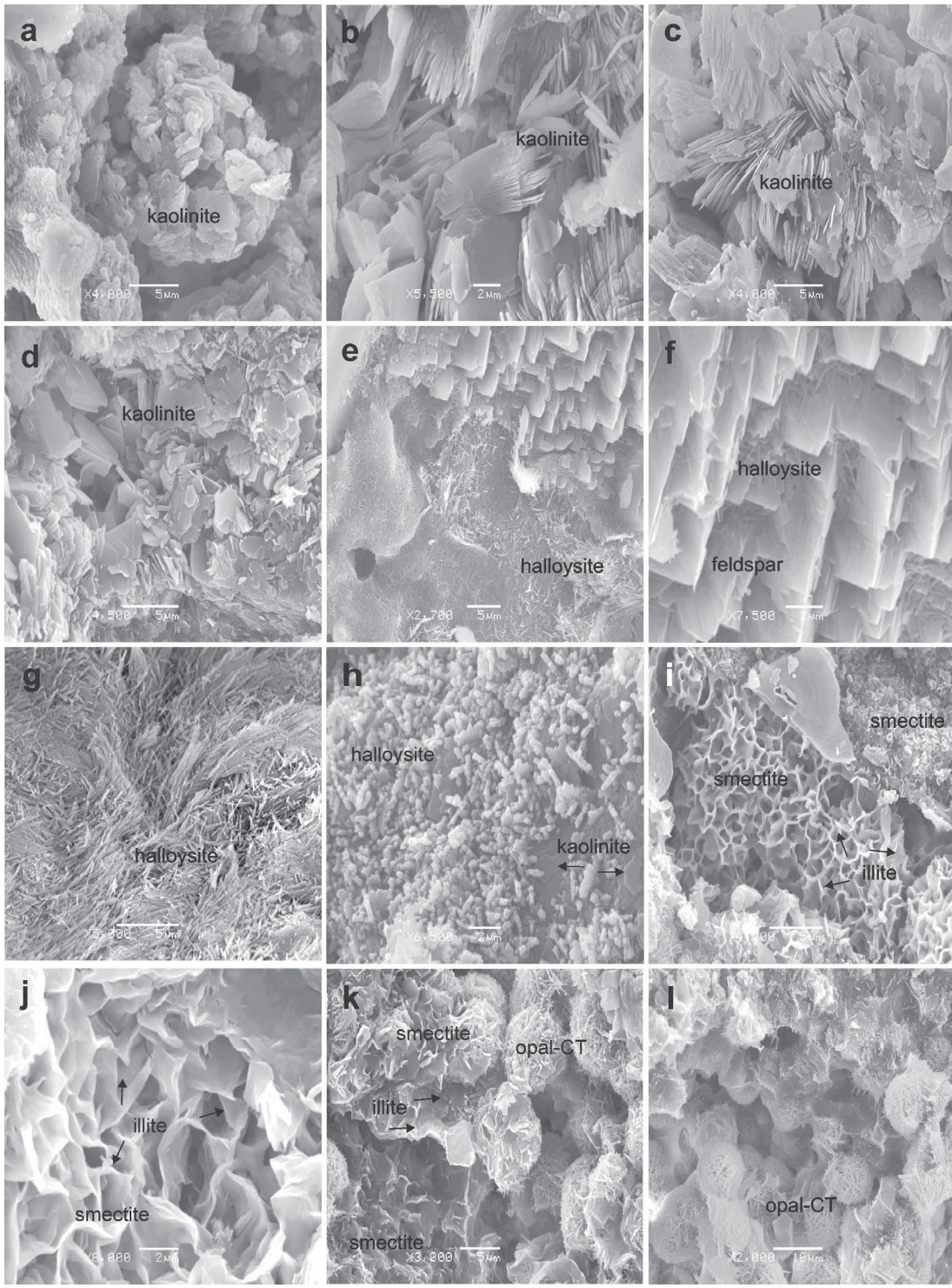

Figure 6. SEM images of (a) development of kaolinite in devitrified volcanic glass (YUY-16); (b) development of kaolinite plates at the edges of altered volcanic materials (KURT-2); (c) book-like kaolinite plates (KURT-2); (d) euhedral hexagonal kaolinite plates in microfracture (KURT-5); (e) relationship between fibrous halloysite and volcanic materials developed *via* flushing of hydrothermal fluid (KURT-2); (f) a close-up view of e; (g) a close-up view of fibrous halloysite (UL-9); (h) relationship between kaolinite plates covered by rod-like halloysite (SAK-5); (i) cornflake-like smectite edging illite fibers developed in a microfracture of finer smectite; smectite-illite-flake-rich volcanic material (AK-10); (j) a close-up view of i; (k) spherical opal-CT edging smectite plates (UL-9); (l) spherical opal-CT in dissolution voids (UL-9).

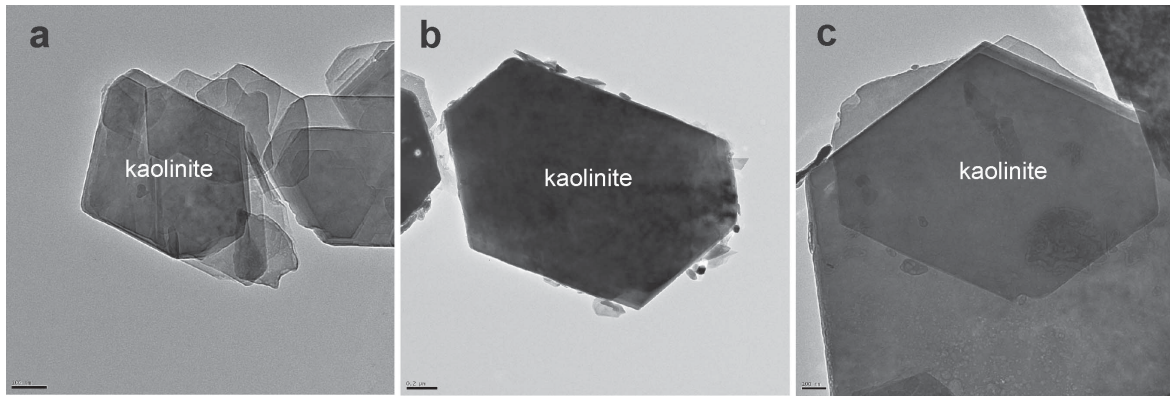

Figure 7. TEM images of: (a–c) hexagonal platy kaolinite crystals (KURT-2, UL-11, YUY-10) of various sizes; scale bar (a,c) = 100 nm; (b) = 0.2 μm.

advances in hydrothermal alteration processes (Table 3; Figure 11). Generally, SiO_2 (except in the kaolinite deposits of Yüylük and Hisarcık), K_2O, NaO, and CaO show evidence of leaching and thus were depleted; Al_2O_3 was enriched (except in the Yağmurlar deposits) during the alteration of K-feldspar, plagioclase, and

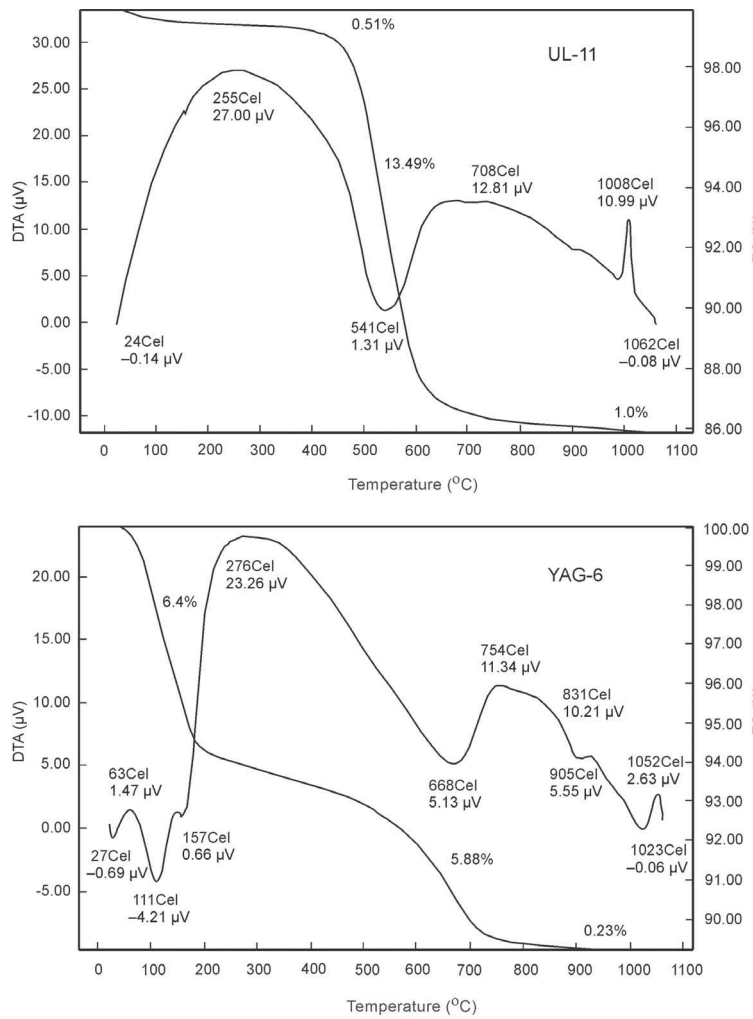

Figure 8. DTA-TG curves for Kütahya kaolinite (UL-11) and smectite (YAG-6) samples.

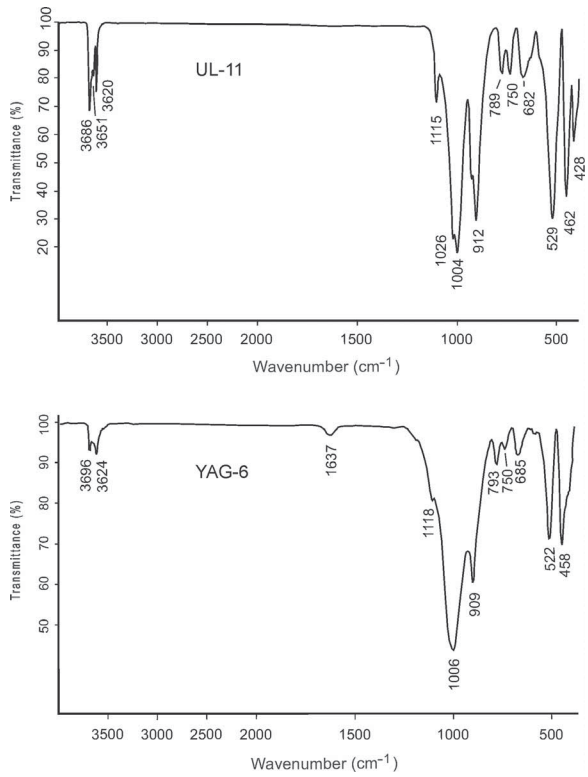

Figure 9. FTIR spectra for Kütahya kaolinite (UL-11) and smectite (YAG-6) samples.

volcanic glasses in the volcanic units. MgO (except in the partially altered Akçaalan deposits) and Fe_2O_3 were depleted by leaching, except in the partially altered Hisarcık and Akçaalan areas where enrichment occurred related to degradation of hornblende and biotite. Thus, increase in the Al/Si ratio and LOI with advancing alteration (from fresh host-rock samples to altered units) indicates kaolinization and smectitization (Tables 2, 3). The large amount of SiO_2 is related to the presence of opal-CT, quartz, chalcedony, and feldspar. K_2O reflects the presence of illite, K-feldspar, and hornblende.

Rb and Ba were depleted by leaching, and Sr (except in the Yağmurlar and Akçaalan deposits) was enriched (Table 3; Figure 11). Degradation of K- and Ca-bearing minerals (such as feldspar) at hydrothermal temperatures resulted in Sr enrichment, and differentiation of K-feldspar and hornblende resulted in the leaching of Rb+Ba and K_2O contents. The increase of Ba in altered relative to the partially altered Hisarcık kaolinite deposit was possibly related to the formation of illite and the substitution of Ba for K. Leaching of Co was related locally to degradation of ferromagnesian phases such as hornblende. Negative Nb and Ti anomalies reflect partial melting of subducted eclogite in upper crustal levels (Ringwood, 1990).

The *REE* were normalized to chondrite values (Figure 12). The *REE* patterns displayed an enrichment of *LREE* [$(La/Sm)_{cn}$ = 3.20–10.91 and $(La/Lu)_{cn}$ = 5.04–96.67]; depletion of *HREE* [$(Gd/Yb)_{cn}$= 0.70–8.58, $(Tb/Yb)_{cn}$= 0.74–4.08, and $(Tb/Lu)_{cn}$= 0.77–4.08]; and negative Eu anomalies [(Eu/Eu*) = 0.50–0.77 and $(Eu/Sm)_{cn}$= 0.36–0.62] in samples from the Yüylük, Hisarcık, Simav, and Gediz kaolinite deposits (Table 2). The $(La/Yb)_{cn}$= 5.03–96.67 ratio revealed enrichment of total *REE* during alteration processes within the volcanites (Roy and Smykatz-Kloss, 2007). The negative Eu anomalies may reflect differentiation of plagioclase and/or K-feldspar based on low *REE* values, and may have developed during progressive hydrothermal alteration (Shikazono *et al.*, 2008; Kadir and Kart, 2009).

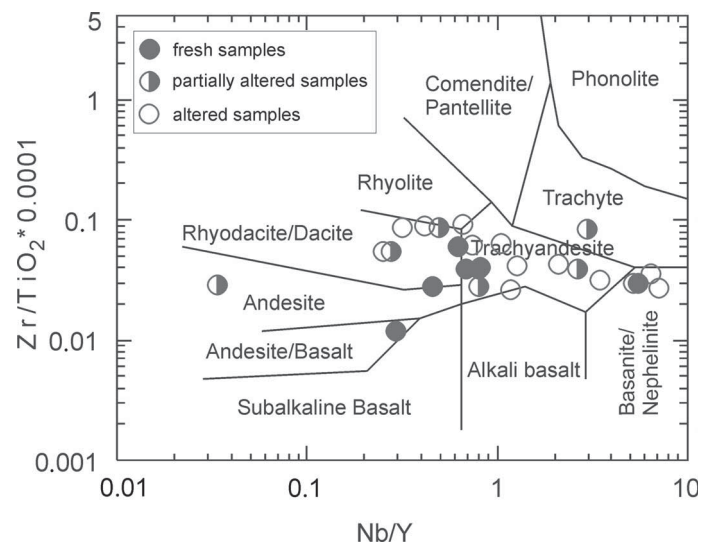

Figure 10. Geochemical discrimination of the Kütahya kaolinite deposits and volcanic-rock samples from the vicinity using a Nb/Y-Zr/TiO_2 immobile-element diagram (Winchester and Floyd, 1977).

Table 2. Major-element (wt.%) and trace-element (ppm) compositions of fresh, partially altered, and highly altered volcanites of the study area (see Table 1 for the mineralogical compositions of the samples).

	Yüylük area					
	Altered				Partially altered	Fresh
%	YUY-10	YUY-16	YUY-19	Average	YUY-35	YUY-11
SiO_2	55.15	47.71	44.55	49.14	69.93	73.24
Al_2O_3	30.93	30.13	38.03	33.03	19.47	9.33
ΣFe_2O_3	0.30	6.67	0.27	2.41	0.4	9.04
MgO	0.07	0.12	0.02	0.07	0.06	0.05
CaO	0.06	0.06	0.04	0.05	0.11	0.06
Na_2O	<0.01	0.02	0.01	0.01	0.04	0.02
K_2O	0.04	0.09	0.08	0.07	0.04	0.14
TiO_2	0.55	0.71	0.93	0.73	0.42	1.31
P_2O_5	0.254	0.465	0.515	0.410	0.20	0.111
MnO	<0.01	<0.01	<0.01	0.01	0.01	<0.01
Cr_2O_3	0.014	0.013	0.035	0.02	0.012	0.007
LOI	12.3	13.8	14.9	13.7	9.1	6.4
Total	99.66	99.72	99.40	99.59	99.76	99.74
Ba	271	282	381	311	117	79
Be	<1	1	<1	1	1	1
Co	2.5	8.8	<0.2	3.8	0.3	1.3
Cs	0.3	0.5	<0.1	0.3	1.2	1.8
Ga	27.1	27.6	39.4	31.4	24.1	15.1
Hf	4.3	6.3	6.9	5.8	3.6	11.9
Nb	14.2	18.3	25.9	19.5	9.8	34.5
Rb	1.5	3.3	0.2	1.7	2.3	9.1
Sn	2	3	4	3	2	7
Sr	2241	3367	5519	3709	1671	420.5
Ta	1.2	1.5	1.7	1.5	1.0	2.8
Th	17.0	24.8	32.5	24.8	12.4	18.2
U	12.8	12.2	9.1	11.4	1.3	17.4
V	180	169	233	194	67	130
W	2.9	4.0	2.3	3.1	1.7	5.5
Zr	147.8	225.7	241.7	205.1	124.8	394
Y	2.0	5.3	22.2	9.8	1.9	6.3
La	36.9	73.3	67.1	59.1	21.4	28
Ce	85.5	174.3	149.4	136.4	34.2	44
Pr	11.66	21.10	18.64	17.1	3.69	3.97
Nd	48.7	85	73	69	13	11.4
Sm	7.24	12.49	12.12	10.60	1.75	1.76
Eu	1.0	1.82	1.94	1.60	0.32	0.35
Gd	2.76	4.96	7.02	4.91	1.42	1.35
Tb	0.24	0.39	0.74	0.46	0.13	0.22
Dy	0.88	1.39	3.98	2.08	0.41	1.32
Ho	0.08	0.17	0.72	0.32	0.07	0.27
Er	0.25	0.54	2.33	1.04	0.14	0.82
Tm	0.04	0.08	0.41	0.18	0.03	0.13
Yb	0.26	0.71	2.62	1.20	0.25	1.10
Lu	0.04	0.10	0.39	0.18	0.04	0.18
Pb	10.5	22.7	10.8	14.7	5	25.5
Zn	3	3	<1	2	2	12
Ni	6.5	24.1	0.9	10.5	2.3	10
Au (ppb)	36	1.6	0.9	12.8	0.5	2.6
Ag	<0.1	<0.1	<0.1	0.1	0.1	<0.1
Mo	0.1	1.0	1.2	0.8	0.2	3.4
Cu	2.1	9.7	3.4	5.1	1.6	27.8
As	1.2	19.8	3.2	8.1	2.8	81.3
Cd	<0.1	<0.1	<0.1	0.1	0.1	<0.1
Sb	0.1	0.4	0.2	0.23	0.1	0.8
ΣREE	195.55	381.35	340.41	305.77	76.85	94.87
$(Eu/Eu^*)_{cn}$	0.68	0.70	0.64	0.67	0.62	0.69
$(Ce/Ce)_{cn}$	0.99	1.05	1.00	1.01	0.79	0.81
$(La/Sm)_{cn}$	3.20	3.69	3.48	3.45	7.69	10.01
$(La/Yb)_{cn}$	96.67	69.74	17.27	61.22	58.00	17.17
$(La/Lu)_{cn}$	96.67	76.27	17.87	63.6	55.66	16.15
$(Eu/Sm)_{cn}$	0.36	0.38	0.42	0.38	0.48	0.52
$(Gd/Yb)_{cn}$	8.58	5.64	2.16	5.46	4.60	0.99
$(Tb/Yb)_{cn}$	4.08	2.42	1.24	2.58	2.30	0.88
$(Tb/Lu)_{cn}$	4.08	2.65	1.28	2.67	2.20	0.83

$Eu/Eu^*=Eu_N/\sqrt{(Sm_N * Gd_N)}$ and $Ce/Ce^*=3Ce_N/(2La_N+Nd_N)$ (Mongelli, 1997), LOI: loss on ignition at 1050ºC.

Table 2 (*contd*.).

	Hisarcık area									
	Altered				Partially altered			Fresh		
%	UL 6	SAK-5	KURT-2	Average	UL-10	SAK-13	Average	UL-23	SAK-26	Average
SiO_2	64.02	62.48	45.01	57.17	61.64	57.62	59.63	67.58	53.04	60.31
Al_2O_3	23.78	23.65	38.59	28.67	14.56	16.06	15.31	15.59	14.4	14.99
ΣFe_2O_3	0.41	1.84	0.36	0.87	5.73	4.78	5.25	2.74	7.53	5.13
MgO	0.17	0.08	0.03	0.09	2.1	2.34	2.22	0.97	4.97	2.97
CaO	0.14	0.22	0.31	0.22	1.01	1.06	1.03	1.66	5.79	3.72
Na_2O	0.01	0.02	0.13	0.05	0.36	0.04	0.2	2.2	2.31	2.25
K_2O	0.09	0.06	0.10	0.08	2.59	0.45	1.52	6.08	6.52	6.3
TiO_2	0.61	0.76	<0.01	0.46	0.5	0.56	0.53	0.51	1.92	1.21
P_2O_5	0.076	0.165	0.148	0.129	0.116	0.11	0.11	0.11	0.56	0.33
MnO	<0.01	<0.01	<0.01	0.01	0.02	0.02	0.02	0.03	0.1	0.06
Cr_2O_3	<0.002	0.004	0.003	0.003	0.004	0.003	0.003	0.002	0.048	0.02
LOI	9.8	10.2	14.9	11.6	11.3	16.8	14.05	2.2	2.4	2.3
Total	99.14	99.44	99.59	99.39	99.95	99.79	99.87	99.69	99.63	99.66
Ba	1579	1958	2621	2052.6	666	398	532	1606	898	1252
Be	<1	<1	<1	1	2	2	2	3	2	2.5
Co	<0.2	7.7	0.5	2.8	5.4	5	5.2	4.1	3.3	3.7
Cs	37.8	15.9	0.5	18.06	66.8	31.2	49	4.7	58.7	31.7
Ga	20	22.6	3.7	15.43	13.7	18.5	16.1	16	13.9	14.95
Hf	6.8	9.4	0.2	5.46	4.32	6.2	5.26	6	6.5	3.25
Nb	17.5	21.6	0.2	13.1	0.91	15.5	8.2	14.2	17.2	15.7
Rb	15.7	6.9	0.7	7.76	2.66	39.7	21.18	203.6	23.1	113.35
Sn	4	5	<1	3.33	0.43	4	2.21	3	3	3
Sr	497.3	905.5	1785	1062.6	2.58	557	279.79	218.6	183.3	200.95
Ta	1.5	1.9	<0.1	1.16	0.4	1.4	0.9	1.3	1.2	1.25
Th	21.8	29.7	9.3	20.26	0.02	25	1.01	19.6	39.4	29.5
U	4.5	9.2	0.4	4.7	4.7	1.9	3.3	9.3	8.7	9
V	82	116	124	82.6	77	50	63.5	60	60	60
W	6.6	3.7	0.5	3.6	8	2.3	5.15	2	2.1	2.05
Zr	217	322.5	5.5	181.6	142.2	216.3	179.25	200.3	227.5	213.9
Y	2.7	10.3	0.8	4.6	26.9	5.9	16.4	20.9	58.5	39.7
La	34.5	41.7	6.8	27.6	27.3	27.5	27.4	33.8	50.5	42.15
Ce	58.4	80.8	12.1	50.43	51.8	50.2	51	62	108.9	85.45
Pr	5.60	9.05	1.34	5.33	6.08	5.38	5.73	7.12	13.14	10.13
Nd	16.9	30.6	3.8	17.1	23.5	19.9	21.7	25.4	49.7	37.55
Sm	1.99	4.45	0.56	2.3	4.48	2.9	3.69	4.54	8.97	6.75
Eu	0.31	0.75	0.08	0.38	0.78	0.41	0.59	0.97	1.82	1.39
Gd	1.25	2.95	0.19	1.46	4.46	2.16	3.31	3.91	7.89	5.9
Tb	0.15	0.48	0.04	0.22	0.76	0.27	0.51	0.65	1.51	1.08
Dy	0.67	2.55	0.19	1.13	4.32	1.47	2.89	3.51	8.96	6.23
Ho	0.11	0.43	0.03	0.19	0.91	0.27	0.59	0.72	1.89	1.30
Er	0.38	1.26	0.09	0.57	2.66	0.84	1.75	2.1	5.96	4.03
Tm	0.06	0.22	0.02	0.1	0.43	0.14	0.28	0.35	1.04	0.69
Yb	0.47	1.45	0.09	0.67	2.58	0.99	1.78	2.22	6.76	8.98
Lu	0.08	0.23	0.03	0.11	0.4	0.16	0.28	0.35	1.04	0.69
Pb	10.1	95.3	2.9	36.1	10.9	15.5	13.2	10.2	6.0	8.1
Zn	9	54	<1	21.3	225	30	127.5	27	15	21
Ni	1.0	38.7	1.7	13.8	12.5	21.1	16.8	4.1	5.5	4.8
Au (ppb)	0.7	<0.5	<0.5	0.56	0.5	1	0.75	<0.5	<0.5	0.5
Ag	<0.1	<0.1	<0.1	0.1	0.1	0.1	0.1	<0.1	<0.1	0.1
Mo	0.3	2.1	0.5	0.96	0.3	0.3	0.3	0.8	<0.1	0.45
Cu	0.8	21	3.2	8.3	4.3	5.7	5	3.8	0.7	2.25
As	117.3	674.9	14.7	268.9	11.5	11.8	11.65	17.2	7.3	6.12
Cd	<0.1	0.2	<0.1	0.13	0.2	0.1	0.15	<0.1	<0.1	0.1
Sb	4.4	5.8	0.7	3.63	9.4	0.9	5.15	0.8	0.5	0.65
Σ*REE*	120.87	176.92	25.36	107.71	130.46	112.59	121.52	147.64	268.08	207.86
$(Eu/Eu^*)_{cn}$	0.60	0.63	0.75	0.66	0.53	0.50	0.51	0.70	0.66	0.68
(Ce/Ce)cn	0.86	0.86	0.89	0.87	0.89	0.88	0.88	0.88	0.98	0.93
(La/Sm)cn	10.91	5.89	7.64	8.14	3.83	5.96	4.89	4.68	3.54	4.11
(La/Yb)cn	49.68	18.76	51.0	39.81	7.13	18.75	12.94	10.26	5.03	7.64
(La/Lu)cn	44.87	18.83	23.58	29.09	7.09	17.88	12.48	10.03	5.04	7.53
(Eu/Sm)cn	0.41	0.44	0.37	0.4	0.46	0.37	0.41	0.56	0.53	0.54
(Gd/Yb)cn	2.15	1.64	1.69	1.82	1.39	1.76	1.57	1.42	0.94	1.18
(Tb/Yb)cn	1.41	1.46	1.95	1.6	1.29	1.32	1.30	1.29	0.98	1.13
(Tb/Lu)cn	1.27	1.41	0.90	1.19	1.29	1.14	1.21	1.26	0.98	1.12

Table 2 (*contd*.).

	Yağmurlar (Simav area)									
	Altered				Partially altered			Fresh		
%	YAG-6	YAG-7	YAG-11	Average	YAG-4	YAG-15	Average	YAG-26	YAG-31	Average
SiO_2	63.79	70.45	67.3	67.18	74.5	72.11	73.30	73.18	76.01	74.59
Al_2O_3	14.28	13.5	13.7	13.82	12.31	14.47	13.39	12.33	9.83	11.08
ΣFe_2O_3	2.03	0.69	0.97	1.23	0.56	0.26	0.41	1.76	2.47	2.03
MgO	2.94	1.65	2.16	2.25	1.40	0.34	0.87	0.75	0.10	0.42
CaO	1.32	0.83	1.1	1.08	0.72	0.31	0.51	0.68	0.10	0.39
Na_2O	0.03	0.02	0.03	0.02	0.03	0.03	0.03	0.89	0.44	0.66
K_2O	0.10	0.10	0.09	0.09	0.11	0.93	0.51	6.35	6.35	6.35
TiO_2	0.28	0.26	0.26	0.26	0.27	0.31	0.29	0.43	0.31	0.37
P_2O_5	0.029	0.037	0.044	0.03	0.067	0.079	0.073	0.075	0.19	0.13
MnO	0.08	0.02	<0.01	0.03	0.02	<0.01	0.15	<0.01	0.02	0.01
Cr_2O_3	<0.002	<0.002	<0.002	0.002	<0.002	<0.002	0.002	0.003	0.002	0.002
LOI	15.6	12.0	13.8	13.8	10.3	10.4	10.3	3.2	3.8	3.5
Total	100.49	99.52	99.46	99.96	100.28	99.23	99.75	99.68	99.67	99.67
Ba	274	90	61	141.6	489	578	533.5	1120	1571	1345.5
Be	2	1	2	1.66	2	<1	1.5	3	2	2.5
Co	0.7	0.9	1.4	1	0.5	0.7	0.6	1.7	1.8	1.75
Cs	41.7	45.2	36.7	41.2	55.2	16.0	35.6	29.8	3.5	16.65
Ga	17.0	15.1	15.2	15.76	14.9	16.7	15.8	15.4	11.4	13.4
Hf	6.8	6.3	6.5	6.5	6.3	7.2	6.75	4.5	3	3.75
Nb	19.9	17.6	17.4	18.3	17.4	21.2	19.3	13.8	9.3	11.55
Rb	14.3	17.3	14.1	15.23	18.4	6.1	7.25	293.5	178.6	236.05
Sn	3	3	3	3	3	3	3	1	2	1.5
Sr	236.8	238.3	220.5	231.86	432.8	510.3	471.5	202.4	493.3	347.85
Ta	1.2	1.2	1.3	1.23	1.2	1.6	1.4	0.9	0.8	0.85
Th	41.3	41.1	39.5	40.63	48.6	27.0	37.8	18.3	11.7	15
U	2.9	7.3	11.3	7.16	8.4	1.1	42.5	3.5	4.6	4.05
V	<8	32	22	20.6	19	22	20.5	52	44	48
W	1.7	2.8	2.7	2.4	3.6	8.0	5.8	7.3	3.7	5.5
Zr	254.3	228.6	227.0	236.63	233.8	256.1	244.95	175.1	120.5	147.8
Y	30.1	42.7	54.6	42.46	35.3	7.1	21.2	16.8	11.6	14.2
La	55.4	65.9	85.8	69.03	155.3	32.1	93.7	47.4	44.5	45.95
Ce	99.0	118.9	170.1	129.3	319.3	43.6	181.45	82.3	59.6	70.95
Pr	11.38	12.47	19.63	14.49	33.06	4.14	18.6	10.14	7.48	8.81
Nd	39.0	45.0	73.5	52.5	105.2	14.5	59.85	35.5	26	30.75
Sm	7.01	7.39	12.40	8.93	15.15	2.02	8.67	4.85	4.09	4.47
Eu	1.31	1.47	2.53	1.77	2.78	0.36	1.57	0.88	0.96	0.92
Gd	5.96	6.43	10.15	7.51	10.68	1.47	6.07	3.62	3.52	3.57
Tb	1.02	1.15	1.74	0.92	1.58	0.22	0.9	0.52	0.47	0.49
Dy	5.63	6.77	9.66	7.35	7.59	1.24	4.41	3.23	2.49	2.86
Ho	1.13	1.37	1.9	1.46	1.37	0.25	0.93	0.64	0.46	0.55
Er	3.47	4.24	5.95	4.55	3.65	0.83	2.24	1.90	1.24	1.57
Tm	0.59	0.72	0.98	0.76	0.64	0.14	0.39	0.29	0.2	0.24
Yb	3.71	4.36	6.38	4.81	4.11	1.10	2.60	2.16	1.32	1.74
Lu	0.57	0.7	1.01	0.76	0.58	0.19	0.38	0.34	0.19	0.26
Pb	13.2	14.6	9.7	12.5	4.5	2.7	3.6	65.3	331.5	198.4
Zn	11	4	7	7.3	6	4	5	182	27	104.5
Ni	1.5	1.3	1.6	1.46	1.4	3.4	2.4	8.7	4.9	6.8
Au (ppb)	0.7	<0.5	0.5	0.56	<0.5	<0.5	0.5	<0.5	17.1	11.05
Ag	<0.1	<0.1	<0.1	0.1	<0.1	<0.1	0.1	<0.1	7	3.55
Mo	0.2	<0.1	<0.1	0.13	<0.1	<0.1	0.1	0.1	10.2	5.15
Cu	0.5	0.2	0.3	0.33	0.4	1.0	0.25	1.2	17.3	87.1
As	26.4	4.9	10.2	13.83	6.2	5.0	5.6	3.2	286.9	145.05
Cd	<0.1	<0.1	<0.1	0.1	<0.1	<0.1	0.1	0.8	0.2	0.5
Sb	2.1	0.5	0.7	2.6	0.9	0.4	0.65	3.9	40.6	22.25
ΣREE	235.18	276.87	401.73	304.59	660.99	102.16	381.57	193.77	152.52	173.14
$(Eu/Eu^*)_{cn}$	0.61	0.65	0.68	0.64	0.66	0.63	0.64	0.64	0.77	1.02
$(Ce/Ce)_{cn}$	0.87	0.88	0.93	0.89	1.00	0.69	0.84	0.83	0.66	0.74
$(La/Sm)_{cn}$	4.97	5.61	4.35	4.97	6.44	10.00	8.22	6.14	6.84	6.49
$(La/Yb)_{cn}$	10.06	10.19	9.06	9.77	25.48	19.68	22.58	14.80	22.74	18.77
$(La/Lu)_{cn}$	10.09	9.78	8.82	9.56	27.81	17.54	22.67	14.49	24.32	19.40
$(Eu/Sm)_{cn}$	0.49	0.52	0.54	0.51	0.48	0.47	0.47	0.48	0.62	0.55
$(Gd/Yb)_{cn}$	1.29	1.18	1.28	1.25	2.09	1.07	1.58	1.35	2.15	1.75
$(Tb/Yb)_{cn}$	1.21	1.16	1.20	1.19	1.69	0.88	1.28	1.06	1.57	1.31
$(Tb/Lu)_{cn}$	2.56	1.11	1.17	1.61	1.84	0.78	1.31	1.03	1.67	1.35

Table 2 (*contd*.).

	Akçaalan (Gediz area)									
	Altered				Partially altered			Fresh		
%	AK-9	AK-10	AK-14	Average	AK-4	AK-7	Average	AK-5	AK-8	Average
SiO_2	64.64	62.82	64.80	64.08	66.34	53.24	59.79	68.52	56.12	62.32
Al_2O_3	18.17	20.77	17.62	18.85	15.82	18.52	17.17	14.71	18.24	16.47
ΣFe_2O_3	0.97	0.90	1.68	1.18	2.54	5.36	3.95	2.50	5.25	3.87
MgO	0.35	0.41	0.41	0.39	1.10	3.87	3.03	0.85	2.84	1.84
CaO	1.82	1.49	1.73	1.68	2.01	5.40	3.70	1.69	5.32	3.50
Na_2O	2.18	1.72	2.3	2.06	2.24	2.58	2.41	1.73	3.07	2.4
K_2O	3.46	2.08	3.40	2.98	5.77	1.45	3.61	7.14	2.13	4.63
TiO_2	0.36	0.46	0.36	0.39	0.36	0.73	0.54	0.34	0.74	0.54
P_2O_5	0.172	0.175	0.089	0.14	0.144	0.289	0.21	0.102	0.289	0.19
MnO	0.03	0.02	0.04	0.03	0.04	0.07	0.05	0.04	0.11	0.07
Cr_2O_3	<0.002	<0.002	<0.002	0.002	<0.002	<0.002	0.002	<0.002	<0.002	0.002
LOI	7.3	8.9	7.0	7.73	3.3	8.3	1.8	2.0	5.6	3.8
Total	99.51	99.70	99.66		99.67	99.83		99.66	99.67	
Ba	1555	1435	1903	1631	1693	1653	1673	1981	1805	1893
Be	4	3	3	3.3	3	2	2.5	5	3	4
Co	0.7	0.8	1.5	0.5	3.9	9.6	6.75	3.8	8.4	6.1
Cs	28.7	40.5	26.4	31.86	14.3	13.2	13.75	14.0	63.7	25.35
Ga	18.2	17.9	17.2	17.76	17.8	18.8	18.3	17.9	19.8	18.85
Hf	6.2	5.3	6.2	5.9	5.6	5.5	5.55	5.5	5.7	5.6
Nb	16.5	14.8	18	16.43	15.7	22.2	18.95	16.3	13.7	15
Rb	211.1	120.5	192.1	174.56	196.9	35.7	116.3	203.8	125.2	164.5
Sn	3	3	3	3	2	3	2.5	3	3	3
Sr	1169	1222	695.1	1028.7	664.3	917.1	790.7	432	900.5	666.25
Ta	1.3	1.1	1.4	5.46	1.2	1.8	2.1	1.1	1.0	1.05
Th	35.4	31.1	37.8	34.76	26.1	22.4	24.25	27.3	23.1	25.2
U	12.8	9.4	9.1	10.43	10.7	5.9	8.3	9.2	5.9	7.55
V	64	92	41	65.66	47	89	68	41	90	65.5
W	12.8	2.9	3.7	6.46	3.0	1.6	2.3	1.8	1.9	1.85
Zr	222.7	188.9	230.4	214	194.3	202.9	198.6	205.4	204.9	205.15
Y	22.3	11.6	17.3	17.06	56.5	27.6	42.05	26.1	30	28.05
La	81.3	65.9	74.2	73.8	47.7	46	46.85	46.4	47.6	47
Ce	161.4	129.9	136.4	142.56	89.3	92.2	90.75	85.9	93.1	89.5
Pr	17.5	14.19	13.75	15.38	9.49	10.40	9.94	9.14	10.72	9.93
Nd	68.6	48.7	45.2	54.16	33.7	40.9	37.3	32.1	42	37.05
Sm	11.94	6.54	6.34	8.27	5.40	6.79	6.09	4.66	7.11	5.88
Eu	2.37	1.31	1.28	1.65	1.19	1.61	1.4	1.05	1.65	1.35
Gd	8.38	4.37	4.53	5.76	5.13	5.97	5.55	4.35	6.13	5.24
Tb	1.03	0.56	0.59	0.72	0.98	0.84	0.91	0.68	0.89	0.78
Dy	4.57	2.78	3.25	3.53	7.32	4.78	6.05	4.27	5.19	4.73
Ho	0.78	0.44	0.63	0.61	1.67	0.97	1.32	0.87	1.01	0.94
Er	2.28	1.29	1.79	1.78	5.47	2.78	4.12	2.71	2.80	2.75
Tm	0.37	0.20	0.31	0.29	0.90	0.45	0.67	0.44	0.45	0.44
Yb	2.57	1.36	2.11	2.01	5.85	2.98	4.41	2.78	2.84	2.81
Lu	0.39	0.19	0.32	0.3	0.86	0.43	0.64	0.41	0.42	0.41
Pb	41.1	13.3	54.6	36.3	30.5	31.1	30.8	29.7	20.7	25.2
Zn	63	72	76	70.3	26	62	44	28	42	35
Ni	1.1	0.7	1.4	1.06	2.3	4.7	3.5	3.3	1.5	2.4
Au (ppb)	4.7	1.1	3.8	3.2	<0.5	10.5	5.5	<0.5	3.2	0.35
Ag	<0.1	<0.1	<0.1	0.1	<0.1	<0.1	0.1	<0.1	<0.1	0.1
Mo	0.5	0.1	0.2	0.26	0.4	0.9	0.65	0.2	0.2	0.2
Cu	2.0	2.7	2.2	2.3	3.5	6.7	5.1	5.0	5.0	5.0
As	4.2	4.1	7.3	5.2	2.5	0.7	1.6	2.9	1.2	2.05
Cd	0.2	0.4	0.2	0.26	<0.1	0.2	0.15	<0.1	<0.1	<0.1
Sb	0.3	0.2	0.2	0.23	<0.1	<0.1	0.1	<0.1	0.1	0.1
ΣREE	363.48	277.73	290.7	310.63	214.96	217.10	216.03	195.76	221.91	208.83
$(Eu/Eu^*)_{cn}$	0.72	0.74	0.73	0.73	0.69	0.77	0.73	0.71	0.76	0.73
$(Ce/Ce)_{cn}$	0.93	0.95	0.91	0.93	0.91	0.93	0.92	0.90	0.91	0.90
$(La/Sm)_{cn}$	4.28	6.33	7.36	5.99	5.55	4.26	4.9	6.26	4.21	5.23
$(La/Yb)_{cn}$	21.33	32.70	23.72	25.91	5.49	10.41	7.95	11.25	11.30	11.27
$(La/Lu)_{cn}$	21.65	36.03	24.10	27.26	5.76	11.11	8.43	11.75	11.77	11.76
$(Eu/Sm)_{cn}$	0.52	0.53	0.53	0.52	0.58	0.62	0.6	0.59	0.61	0.60
$(Gd/Yb)_{cn}$	2.63	2.59	1.73	2.31	0.70	1.61	1.15	1.26	1.74	1.5
$(Tb/Yb)_{cn}$	1.76	1.81	1.23	1.6	0.74	1.24	0.99	1.07	1.38	1.22
$(Tb/Lu)_{cn}$	1.79	2.00	1.25	1.68	0.77	1.32	1.04	1.12	1.43	1.27

Ce/Ce* values of fresh, partially altered, and altered samples vary from 0.66 to 1.05, revealing negative Ce anomalies; these anomalies may be related to the fractionation of the mineral zircon under oxidizing-acidic fluid conditions (Fulignati *et al.*, 1999; Karakaya, 2009).

Mineral chemistry

The structural fomulae of purified clay fractions from the highest-purity kaolinite and smectite samples were calculated from the average chemical analysis values (Table 4), yielding the following for kaolinite and smectite, respectively:

$(Si_{3.67}Al_{0.33})(Al_{3.72}Fe_{0.04}Mg_{0.01}Ti_{0.09}Mn_{0.001})$
$(Ca_{0.01}Na_{0.02}K_{0.15}P_{0.09})O_{10}(OH)_8$;
$(Si_{7.69}Al_{0.31})(Al_{2.88}Fe_{0.45}Mg_{0.59}Ti_{0.05}Mn_{0.002})$
$(Ca_{0.34}Na_{0.013}K_{0.1}P_{0.02})O_{20}(OH)_4$.

The tetrahedral sites of both kaolinite and smectite were filled mainly by Si but this was partially substituted by traces of Al in kaolinite samples YUY-19 and KURT-2 and smectite sample SAK-24. Al was the dominant cation in the octahedral site, accompanied by accessory to trace amounts of Fe(III), Ti, Mg, and Mn that replaced some of the octahedral Al.

The SiO_2/Al_2O_3 ratio in pure Kütahya kaolinite samples varied between 0.78 and 1.36; this result is

Table 3. Mass gains and losses for the Kütahya area samples (compositional values for the oxides are in wt.% and other elements in ppm, and mass changes for them are in g/100 g rock and in ppm/100 g rock, respectively).

	Yüylük kaolinite deposit				Hisarcık kaolinite deposit			
	Partially altered samples (n = 1)		Altered samples (n = 3)		Partially altered samples (n = 1)		Altered samples (n = 3)	
	RC	ΔC_i	RC	ΔC_i	RC	ΔC_i	RC	ΔC_i
SiO_2	217.93	144.69	94.4	21.16	71.15	10.84	67.33	7.02
Al_2O_3	61.47	52.14	63.45	54.12	18.26	3.27	33.76	18.77
ΣFe_2O_3	1.26	−7.78	4.63	−4.41	6.26	1.13	1.02	−4.1
MgO	0.19	0.14	0.13	0.08	2.64	−0.32	0.1	−2.86
CaO	0.35	0.29	0.09	0.03	1.22	−2.49	0.25	−3.46
Na_2O	0.13	0.11	0.02	−0.12	0.23	−2.01	0.05	−2.19
K_2O	0.01	−0.12	0.13	−0.01	1.81	−4.48	0.09	−6.2
TiO_2	1.33	0.02	1.4	0.09	0.63	−0.57	0.54	−0.66
P_2O_5	0.63	0.52	0.79	0.68	0.13	−0.19	0.15	−0.17
Total		190.12		71.74		5.18		6.15
Ba	369.38	290.38	597.4	518.4	634.83	−617.16	2417.68	1165.68
Co	0.95	−0.35	7.3	6	6.2	2.5	3.29	−0.4
Cs	3.79	1.99	0.58	−1.22	58.47	26.77	21.27	−10.42
Ga	76.08	60.98	60.32	45.22	19.21	4.26	18.17	3.22
Hf	11.37	−0.53	11.14	−0.76	6.27	3.02	6.43	3.18
Nb	30.94	−3.56	37.5	2.96	9.78	−5.91	15.43	−0.26
Rb	7.26	−1.84	3.27	−5.83	25.27	−88.07	9.14	−104.2
Sr	5275.43	4854.9	7125	6704.5	333.87	132.92	1251.59	1050.64
Ta	3.16	0.36	2.88	0.08	1.07	−0.17	1.36	0.11
Th	39.15	20.95	47.64	29.4	1.2	−28.29	23.86	−5.63
U	4.1	−13.3	21.9	4.5	3.93	−5.06	5.53	−3.46
V	211.52	81.52	372.7	242.7	75.77	15.77	97.29	37.29
W	5.37	−0.13	5.96	0.46	6.14	4.09	4.24	2.19
Zr	394	0	394	0	213.9	0	213.9	0
Y	6	−0.3	18.82	12.52	19.57	−20.12	5.41	−34.28
La	67.6	39.6	113.53	85.53	32.69	−9.45	32.5	−9.64
Ce	108	64	262.02	218.02	60.85	−24.59	59.39	−26.06
Pr	11.65	7.68	32.85	28.9	6.83	−3.29	6.27	−3.85
Nd	41.04	29.64	132.55	121.15	25.89	−11.65	20.14	−17.4
Sm	5.52	3.76	20.36	18.6	4.4	−2.34	2.7	−4.04
Eu	1.01	0.66	3.07	2.72	0.70	−0.68	0.44	−0.94
Gd	4.48	3.13	9.43	8.08	3.94	−1.95	1.71	−4.18
Tb	0.41	0.19	0.88	0.66	0.60	−0.47	0.25	−0.82
Dy	1.29	−0.03	3.99	2.67	3.44	−2.78	1.33	−4.89
Ho	0.22	−0.05	0.61	0.34	0.70	−0.59	0.22	−1.07
Er	0.44	−0.38	1.99	1.17	2.08	−1.94	0.67	−3.35
Tm	0.09	−0.04	0.34	0.21	0.33	−0.35	0.11	−0.57
Yb	0.79	−0.31	2.3	1.2	2.12	−6.85	0.78	−8.19
Lu	0.13	−0.05	0.34	0.16	0.33	−0.35	0.12	−0.56
Total *REE*		147.8		489.39		−67.28		−85.56

n: number of samples, RC: reconstructed compositions, ΔC_i: net mass changes

Table 3 (*contd*.).

	Yağmurlar kaolinite deposit (Simav area)				Akçaalan kaolinite occurrence (Gediz area)			
	Partially altered samples (n = 2)		Altered samples (n = 3)		Partially altered samples (n = 2)		Altered samples (n = 3)	
	RC	ΔC_i	RC	ΔC_i	RC	ΔC_i	RC	ΔC_i
SiO_2	44.22	−30.36	41.96	−32.62	61.76	−0.55	61.42	−0.89
Al_2O_3	8.07	−3.0	8.63	−2.44	17.73	1.26	18.07	1.6
ΣFe_2O_3	0.24	−1.78	0.76	−1.26	4.08	0.21	1.13	−2.73
MgO	0.52	0.1	1.4	0.98	3.12	1.28	0.37	−1.46
CaO	0.3	−0.08	0.67	0.28	3.82	0.32	1.61	−1.88
Na_2O	0.01	−0.64	0.01	−0.64	2.48	0.08	1.97	−0.42
K_2O	0.3	−6.04	0.05	−6.3	3.72	−0.9	2.85	−1.77
TiO_2	0.17	−0.19	0.16	−0.2	0.55	0.01	0.37	−0.16
P_2O_5	0.04	−0.08	0.01	−0.11	0.21	0.02	0.13	−0.05
Total		−42.07		−42.31		1.73		−7.76
Ba	321.9	−1023.59	88.44	−1257.05	1728.17	−164.82	1563.54	−329.45
Co	0.36	−1.38	0.62	−1.12	6.97	0.87	0.47	−5.62
Cs	21.48	4.83	25.73	9.08	1.74	−23.6	30.54	5.19
Ga	9.53	−3.86	9.84	−3.55	18.9	0.05	17.02	−1.82
Hf	4.07	0.32	4.05	0.3	5.73	0.13	5.65	0.05
Nb	11.64	0.09	0.89	−10.65	1.95	−13.04	15.75	0.75
Rb	4.37	−231.67	9.51	−5.71	120.13	−44.36	167.34	2.84
Sr	284.49	−63.35	144.82	−203.02	816.77	150.52	986.15	319.9
Ta	0.84	−0.005	0.004	−0.84	2.16	1.11	5.23	4.18
Th	22.8	7.8	25.37	10.37	25.04	−0.15	33.32	8.12
U	25.64	21.59	4.47	0.42	8.57	1.02	9.99	2.44
V	12.36	−35.63	12.86	−35.13	70.24	4.74	62.94	−2.55
W	3.49	−2.0	1.49	−4.0	2.37	0.52	6.19	4.34
Zr	147.8	0	147.8	0	205.15	0	205.15	0
Y	12.79	−1.4	26.52	12.32	43.43	15.38	16.35	−11.69
La	56.53	10.58	43.11	−2.83	48.39	1.39	70.74	23.74
Ce	109.48	38.53	80.76	9.81	93.74	4.24	136.66	27.16
Pr	11.22	2.41	9.05	0.24	10.26	0.33	14.74	4.81
Nd	36.11	5.36	32.73	2.04	38.53	1.48	51.92	14.87
Sm	5.23	0.76	5.57	1.1	6.29	0.41	7.92	2.04
Eu	0.94	0.02	1.1	0.18	1.44	0.09	1.58	0.23
Gd	3.66	0.09	4.69	1.12	5.73	0.49	5.52	0.28
Tb	0.54	0.05	0.57	0.08	0.94	0.16	0.69	−0.08
Dy	2.66	−0.19	4.59	1.73	0.14	−4.58	3.38	−1.34
Ho	0.56	0.01	0.91	0.36	1.36	0.42	0.58	−0.35
Er	1.35	−0.21	2.84	1.27	4.25	1.5	1.7	−1.04
Tm	0.23	−0.004	0.47	0.23	0.69	0.25	0.27	−0.16
Yb	1.56	−0.17	3.0	1.26	4.55	1.74	1.92	−0.88
Lu	0.22	−0.03	0.47	0.21	0.66	0.25	0.28	−0.12
Total *REE*		57.2		16.8		8.17		69.88

consistent with the ideal SiO_2/Al_2O_3 ratio (0.992 to 1.082) for kaolinite (Jepson and Rowse, 1975). The $(Na_2O+K_2O)/(CaO+MgO)$ ratio of smectite was 0.15, indicating a Ca-montmorillonitic character (Ece and Yüce, 1999).

The chemical index of alteration (CIA) for these kaolinites varied between 90.65 and 96.58 in samples YUY-10, YUY-19, and KURT-2, and 82.64 in smectite sample SAK-24 (Table 4). The CIA values for secondary clay minerals kaolinite, gibbsite, and chlorite, were 100; illite and smectite values were 70−85 (Nesbitt and Markovics, 1997). These values show that Ca and Na were depleted from the environment during the alteration processes.

Stable-isotope geochemistry of the Kütahya kaolinites and smectites

The oxygen- and hydrogen-isotopic compositions of kaolinite (YUY-10, YUY-19, YUY-20, UL-11, KURT 2) and smectite (YAG-6, UL-9, SAK-24) samples taken from the Yüylük, Hisarcık, and Yağmurlar kaolinite deposits (Table 5, Figure 13) indicated that the $\delta^{18}O$ and δD values of kaolinites ranged from 7.8 to 12.7‰ and from −54 and −83‰, respectively. The $\delta^{18}O$ and δD values of smectites ranged from 17.4 to 20.2‰ and from −82 and −92‰, respectively. The isotopic data for kaolinite and smectite samples fell to the left of the supergene/hypogene line and plotted close to primary magmatic H_2O, indicating that the Kütahya kaolinites

Table 4. Chemical compositions (wt.%) and structural formulae for purified kaolinitic and smectitic samples.

	Kaolinite				Smectite
%	YUY-10	YUY-19	KURT-2	Average	SAK-24
SiO_2	44.46	43.32	29.02	38.93	54.93
Al_2O_3	32.59	37.52	37.33	35.81	19.47
ΣFe_2O_3	1.04	0.44	0.37	0.61	4.14
MgO	0.16	0.02	0.03	0.07	2.79
CaO	0.16	0.05	0.12	0.11	2.18
Na_2O	0.02	0.02	0.23	0.09	0.05
K_2O	0.11	0.12	3.06	1.09	0.57
TiO_2	2.80	1.01	0.08	1.29	0.53
P_2O_5	1.52	0.78	1.13	1.14	0.21
MnO	0.01	0.01	0.01	0.01	0.02
Cr_2O_3	0.032	0.042	0.006	0.02	0.004
LOI	15.1	15.5	27.0	19.2	14.8
Total	99.77	99.88	99.90	99.85	99.86
CIA	90.65	96.58	92.88		82.64
SiO_2/Al_2O_3	1.36	1.15	0.78	1.09	
Tetrahedral					
Si	4.0	3.86	3.15	3.67	7.69
Al		0.14	0.85	0.33	0.31
Octahedral					
Al	3.46	3.80	3.90	3.72	2.88
Fe	0.07	0.03	0.03	0.04	0.45
Mg	0.02	0.003	0.005	0.009	0.59
Ti	0.19	0.07	0.007	0.09	0.05
Mn	0.0005	0.0008	0.001	0.0007	0.0025
Interlayer					
Ca	0.02	0.005	0.014	0.013	0.34
Na	0.003	0.003	0.05	0.018	0.013
K	0.01	0.01	0.43	0.15	0.1
P	0.12	0.06	0.1	0.09	0.024
TC	0.0	0.14	0.85	0.33	0.31
OC	0.60	0.22	0.17	0.33	0.62
TOT	0.60	0.36	1.02	0.66	0.93
IC	0.65	0.32	1.00	0.66	0.91

TC: tetrahedral charge, OC: octahedral charge, TOT: total charge, IC: interlayer charge.

and smectites developed by means of hydrothermal-alteration processes (Sheppard and Gilg, 1996; Gilg *et al.*, 2003) (Figure 13). The isotopic values are consistent with thermal waters of Kütahya, which have $\delta^{18}O$ values that vary between −7.3 and −10.7‰, δD values ranging from −48.4 to −69.4‰, and which plot close to the meteoric-water line (Burçak *et al*., 2007). The isotopic data for kaolinite samples shifted to smaller δD and greater δO values compared to smectitic samples outward from the kaolinization zone, possibly controlled by local hydrothermal temperature changes and/or large degrees of fractionation between liquid and vapor during the crystallization of these minerals (Faure, 1986).

The calculated temperatures of formation for kaolinite samples using their $\delta^{18}O$ values ($\delta^{18}O$ = 1.5‰) and the isotopic-fractionation factor (α) between kaolinite and water (expressed by 1000 ln $\alpha = 2.76*10^6/T^2-6.75$) yielded the range 119.1−186.9ºC (Campbell *et al.*, 1988; Sheppard and Gilg, 1996) (Table 5). The formation temperature for smectite using the $\delta^{18}O$ values and α between smectite and water (expressed by 1000 ln $\alpha = 2.58*10^6/T^2-4.19$) yielded a range of 61.8−84.5ºC (Yeh and Savin 1977; Savin and Lee, 1988).

DISCUSSION

Widespread kaolinite deposits that occur in the Yüylük, Hisarcık, Simav, and Gediz areas (Kütahya, western Anatolia) developed by hydrothermal alteration of volcanic units related to the Middle−Late Miocene and Pliocene volcanic and tectonic regime of the region. The volcanic units consist of rhyolite, dacite, trachyte, trachyandesite, andesite, andesitic basalt, and pyroclastic rocks. Hydrothermal alteration of some of the rhyoda-

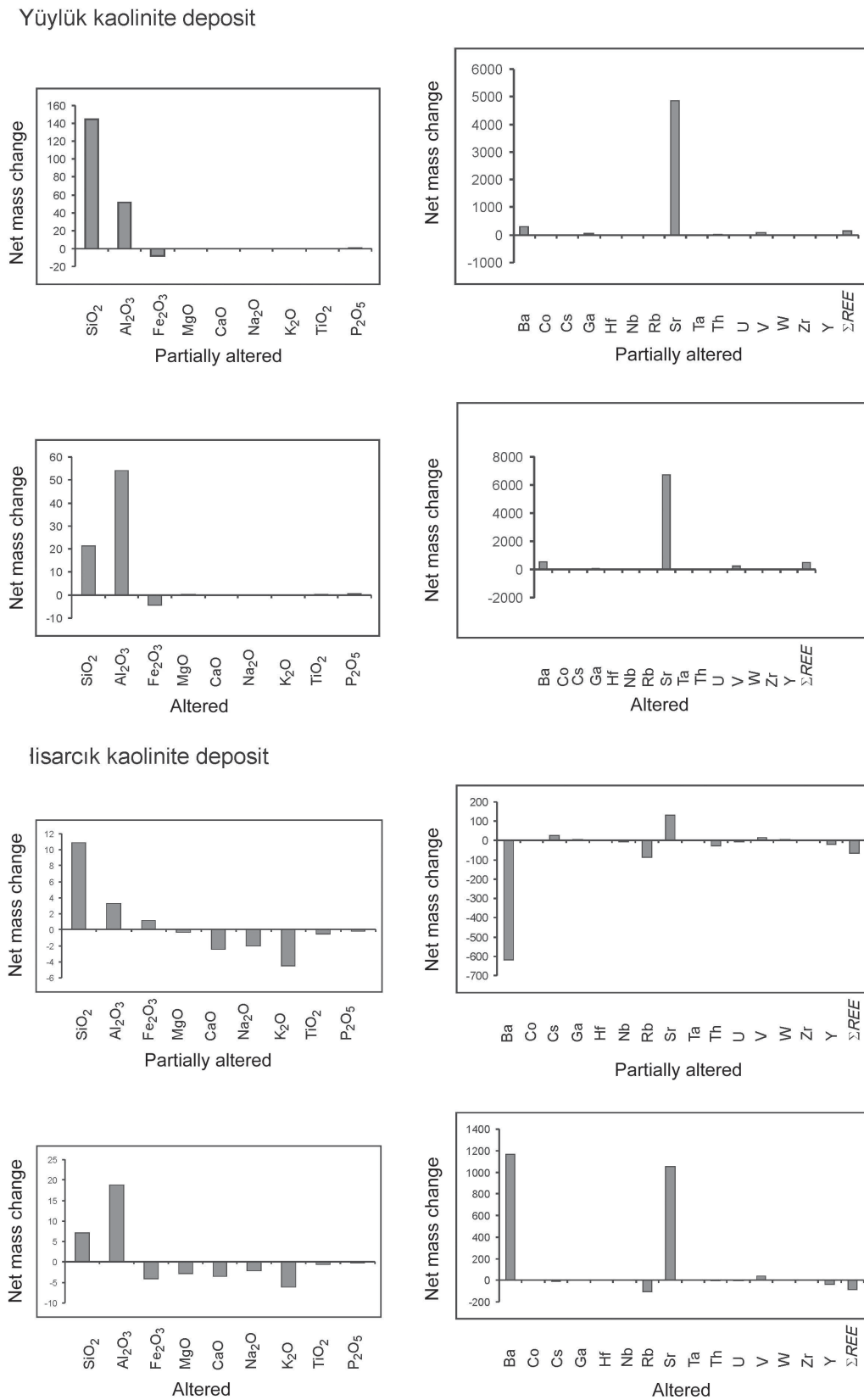

Figure 11 (*this and facing page*). Mass changes of major elements (g) and trace elements (ppm) within the study area.

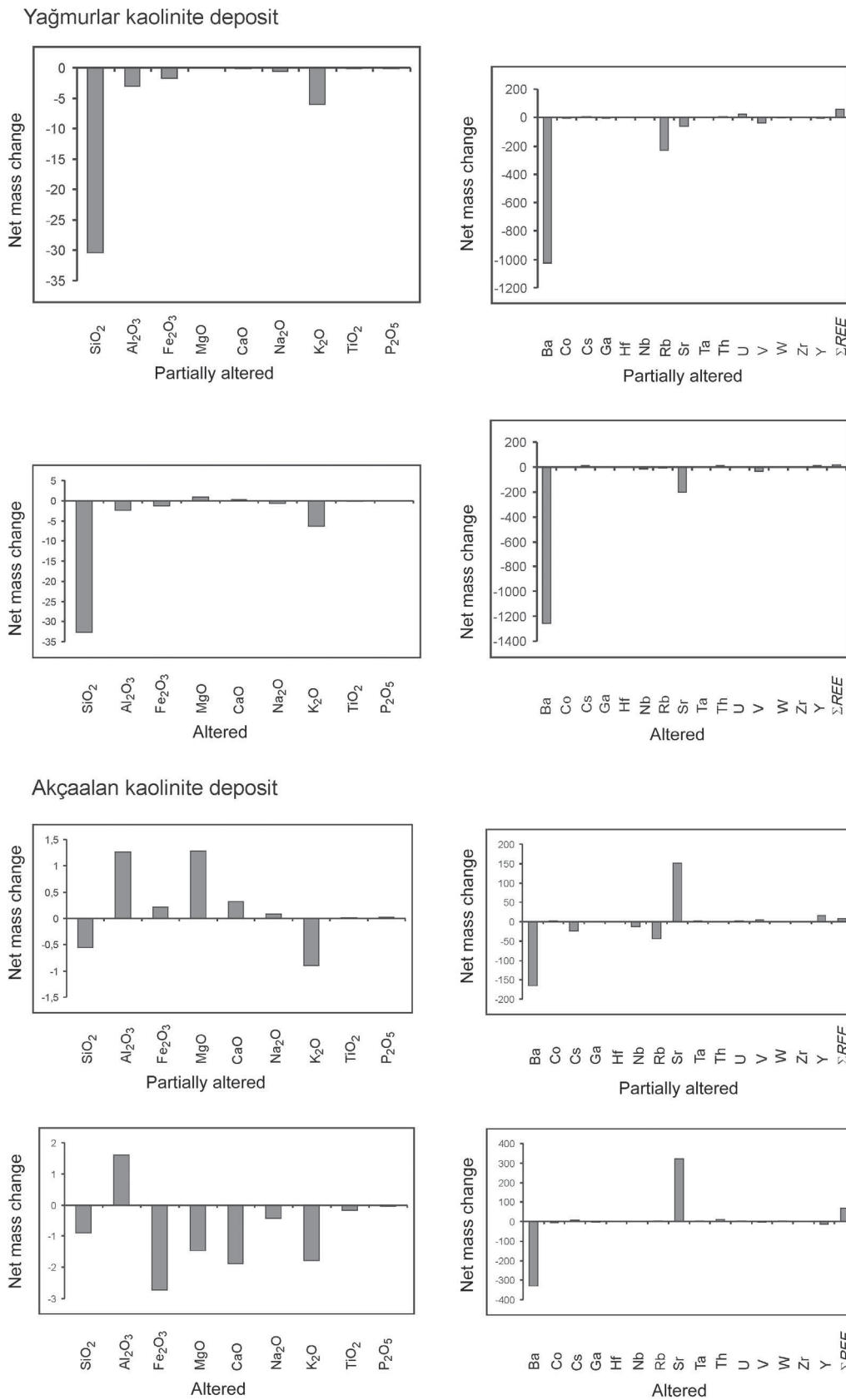
Yağmurlar kaolinite deposit
Net mass change
0
-5
-10
-15
-20
-25
-30
-35
SiO2
Al2O3
Fe2O3
MgO
CaO
Na2O
K2O
TiO2
P2O5
Partially altered
Net mass change
200
0
-200
-400
-600
-800
-1000
-1200
Ba
Co
Cs
Ga
Hf
Nb
Rb
Sr
Ta
Th
U
V
W
Zr
Y
ΣREE
Partially altered
Net mass change
5
0
-5
-10
-15
-20
-25
-30
-35
SiO2
Al2O3
Fe2O3
MgO
CaO
Na2O
K2O
TiO2
P2O5
Altered
Net mass change
200
0
-200
-400
-600
-800
-1000
-1200
-1400
Ba
Co
Cs
Ga
Hf
Nb
Rb
Sr
Ta
Th
U
V
W
Zr
Y
ΣREE
Altered
Akçaalan kaolinite deposit
Net mass change
1,5
1
0,5
0
-0,5
-1
-1,5
SiO2
Al2O3
Fe2O3
MgO
CaO
Na2O
K2O
TiO2
P2O5
Partially altered
Net mass change
200
150
100
50
0
-50
-100
-150
-200
Ba
Co
Cs
Ga
Hf
Nb
Rb
Sr
Ta
Th
U
V
W
Zr
Y
ΣREE
Partially altered
Net mass change
2
1
0
-1
-2
-3
SiO2
Al2O3
Fe2O3
MgO
CaO
Na2O
K2O
TiO2
P2O5
Altered
Net mass change
400
300
200
100
0
-100
-200
-300
-400
Ba
Co
Cs
Ga
Hf
Nb
Rb
Sr
Ta
Th
U
V
W
Zr
Y
ΣREE
Altered

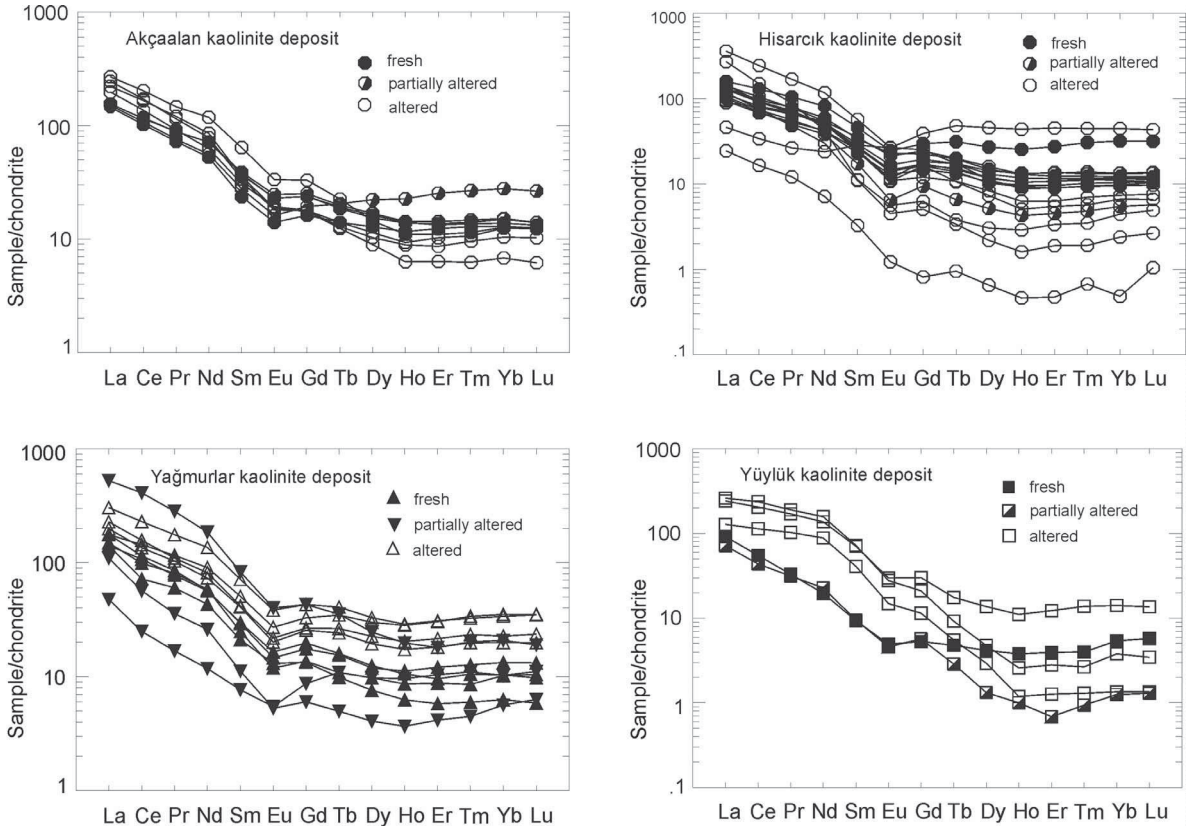

Figure 12. Chondrite-normalized *REE* patterns (Taylor and McLennan, 1985) for kaolinite and related volcanites of the Kütahya area.

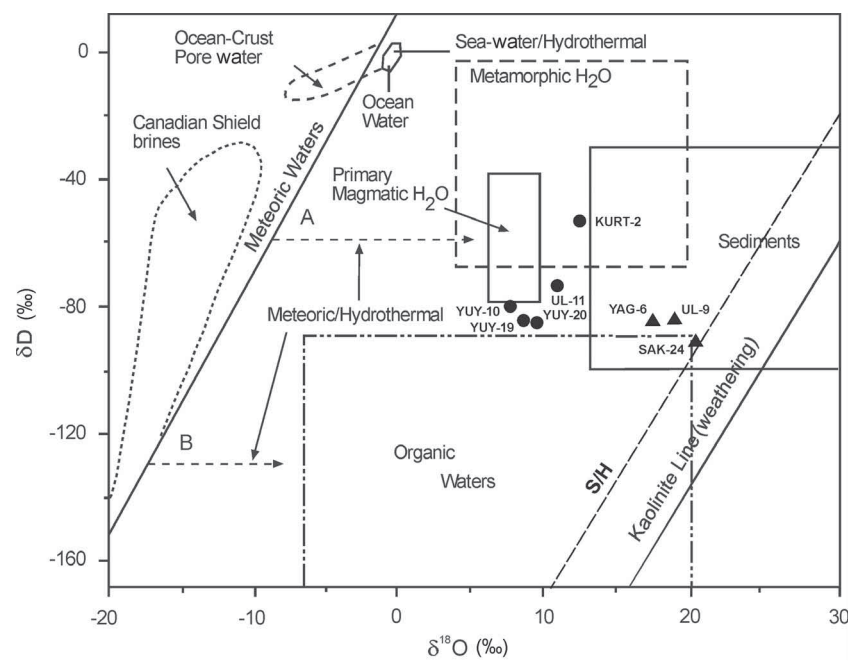

Figure 13. δD *vs.* $\delta^{18}O$ plot showing isotopic compositions of kaolinite (YUY-10, YUY-19, YUY-20, UL-11, KURT-2) and smectite (UL-9, SAK-24, YAG-6) from the Kütahya kaolinite deposits (Sheppard, 1986). The line for kaolinite weathering is from Savin and Epstein (1970), and the line for supergene/hypogene (S/H) is from Sheppard *et al.* (1969).

Table 5. Oxygen- and hydrogen-isotope compositions of clay minerals from the Kütahya kaolinite deposits, with calculated temperatures.

Sample	Mineral	Yield (%)	$\delta^{18}O$ V-SMOV (‰)	Wt.% H_2O	δD V-SMOV (‰)	Formation temp.* (ºC)
YUY-10	kaolinite	14.4	7.8	13.1	−81	186.9
YUY-19	kaolinite	15.5	9	14.9	−83	167.1
YUY-20	kaolinite	14.9	9.8	13.6	−83	155.2
UL-11	kaolinite	16.7	10.9	14.7	−73	140.4
KURT-2	kaolinite	15	12.7	15	−54	119.1
UL-9	smectite	14.8	18.8	9.1	−82	72.6
SAK-24	smectite	14.2	20.2	9.9	−88	61.8
YAG-6	smectite	15.5	17.4	11.4	−92	84.5

* Formation temperatures were calculated assuming $\delta^{18}O_{water}$ = 1.5‰ (Campbell *et al.*, 1988).

cite, dacite, andesite, and trachyandesite units resulted in the development of kaolinite deposits in the Kütahya area.

Acidic hydrothermal solutions flushing along faults and fractures during or following volcanic activity resulted in kaolinization of feldspar and volcanic glass in the volcanic units. These kaolinite deposits contain vertical or subvertical silica and Fe-Ti-(oxyhydr)oxide (pyrite, goethite/lepidocrocite, hematite, and rutile) veins which decrease or disappear upward. Mineralogical zonation from the kaolinite deposits outward generally is: kaolinite ± smectite + illite + opal-CT + feldspar; feldspar + kaolinite + quartz + smectite + illite; quartz + feldspar + volcanic glass. Kaolinite predominates in the centers of the deposits, and smectite and illite increase laterally. In addition, clay minerals are accompanied by calcite, chalcedony, garnet, and pumice fragments. Mineralogical zonation, Fe (oxyhydr)oxide veins, silicification, and local brecciation suggest that these kaolinite deposits developed under the influence of hydrothermal activity (Inoue, 1995; Meunier, 2005; Kadir and Akbulut, 2009; Kadir and Kart, 2009). These results are also supported by the presence of pyrite, goethite/lepidocrocite, hematite, and trace amounts of rutile determined using reflected-light microscopy of silicified, Fe oxidized, and altered samples.

Leaching of excess silica during and following hydrothermal alteration of the volcanic rocks resulted in the precipitation of siliceous caps above the Saklar, Kurtdere, Yağmurlar, and Akçaalan kaolinite deposits (Lavery, 1985; Sayın, 2007).

Textural and micromorphological determinations revealed that sanidine has been sericitized, plagioclase phenocrysts were zoned, and biotite and hornblende have been partially or completely opacitized and chloritized. Feldspars have been re-degraded, and coexist locally with kaolinite at the edges of the feldspars, smectite-illite, opal-CT, and chalcedony, suggesting a dissolution-precipitation mechanism. The leaching of K_2O, CaO, Fe_2O_3, Rb+Ba, and Co, the enriching of Sr, the depletion of *HREE* relative to *LREE*, and the presence of negative Eu anomalies also suggest that alteration of plagioclase, sanidine, hornblende, and glass shards (volcanogenic components) resulted in an increase in the $(Al_2O_3)/(Na_2O+CaO+K_2O)$ ratio, which favored precipitation of kaolinite under acidic environmental conditions *via* a hydrothermal flux in an open hydrologic system (Shikazono *et al.*, 2008; Felhi *et al.*, 2008). Furthermore, linkage between volcanogenic components and authigenic smectite also suggests that dissolution of feldspar and volcanic glass favored the formation of smectite in an alkaline environment via relative increase of $SiO_2+Fe_2O_3+MgO+Na_2O+CaO+K_2O$ and decrease of $Al_2O_3+TiO_2$ in a pore-water flux within volcanic units outward from the kaolinite deposits. The hydrothermal kaolinization process may have developed following sericitization of K-feldspar within the volcanic units (Parry *et al.*, 1984). Dissolution of feldspar and hornblende may have resulted in excess K, causing conversion of smectite to illite under alkaline environmental conditions in a pore-water flux system (Braide and Huff, 1986; Erhenberg, 1991; Meunier and Velde, 2004; Ziegler, 2006).

Micromorphologically, the occurrence of trace fibrous and short rod-like authigenic halloysite in kaolinite-rich samples KURT-2 and SAK-5 and the coating of platy kaolinite by rod-like halloysite indicated local alteration of volcanic materials and authigenic precipitation of halloysite; the dehydration of halloysite-to-kaolinite possibly developed over time (Huang, 1974; Churchman and Gilkes, 1989; Arslan *et al.*, 2006).

The sharp peaks at 7.2 and 3.57 Å and non-basal reflections, ideal DTA-TG curves, sharp bands in FTIR spectra, pseudohexagonal to hexagonal forms, and SiO_2/Al_2O_3 ratios from 0.78 to 1.36 in purified kaolinite samples indicated a well crystallized kaolinite (Jepson and Rowse, 1975; Kadir and Karakaş, 2002; Saikia *et al.*, 2003). The CIA values between 90.65 and 96.58 for kaolinite and 82.64 for smectite in pure clay samples are

compatible with international standards (Nesbitt and Markovics, 1997).

The calculated temperature of formation for the Kütahya kaolinite, using $\delta^{18}O$ values, was 119.1−186.9ºC, consistent with thermal-water reservoir temperatures of 38−232ºC from western Anatolia, as reported by Mutlu and Güleç (1998). The $\delta^{34}S$ from the Şaphane alunite deposit (Kütahya) also revealed a magmatic origin for sulfur (Mutlu *et al.*, 2005). Using $\delta^{18}O$ values, the formation temperature for the Kütahya smectite was 61.8−84.5ºC; this temperature range also supports the suggestion of a hydrothermal mechanism and lateral decrease in temperature from kaolinite in the center to smectite outward from the kaolinite deposits.

CONCLUSION

The Kütahya kaolinite deposits formed by hydrothermal alteration of dacite, andesite, and tuffs, products of Neogene volcanism which were controlled by tectonic activity. These alteration processes resulted in mineralogical zonation outward from the main kaolinite deposits, as follows: kaolinite ± smectite + illite + opal-CT + feldspar; feldspar + kaolinite + quartz + smectite + illite; quartz + feldspar + volcanic glass. The decrease in the $(Al_2O_3+TiO_2)/(SiO_2+Fe_2O_3+MgO+Na_2O+CaO+K_2O)$ ratio from the center of the kaolinite deposit outward also supported the hydrothermal-zonation hypothesis, consistent with the calculated temperatures of formation for the Kütahya kaolinites and smectites (119.1−186.9ºC and 61.8−84.5ºC, respectively).

On the basis of altered feldspar edged by kaolinite, enrichment of Sr, depletion of Rb+Ba, a negative Eu anomaly, and depletion of the *HREE* relative to the *LREE*, kaolinite is suggested to have formed by a dissolution-precipitation mechanism under acidic environmental conditions in an open hydrologic system, and outward, smectite formed authigenically in an alkaline environment controlled by pore-water flux. Similar alkaline conditions resulted in the conversion of smectite to illite in the presence of excess K.

ACKNOWLEDGMENTS

The study was supported financially by the Scientific Research Projects Fund of Eskişehir Osmangazi University in the framework of Project 200715009, and consists of further work on the second author's MSc study, supervised by the first author. The authors are indebted to anonymous reviewers for their careful and constructive reviews, which significantly improved the quality of the paper. They are also grateful to Professor Warren D. Huff (University of Cincinnati, USA) and Professor Joseph W. Stucki (University of Illinois, USA) for their insightful editorial comments and suggestions, and also for detailed reviews and suggestions on an early draft of the manuscript by Professor Huff.

REFERENCES

Arslan, M., Kadir, S., Abdioğlu, E., and Kolaylı, H. (2006) Origin and formation of kaolin minerals in saprolite of Tertiary alkaline volcanic rocks, Eastern Pontides, NE Turkey. *Clay Minerals*, **41**, 597−617.

Akdeniz, N. and Konak, N. (1979a) *Simav-Emet-Tav*şanlı-Dursunbey-Demirci yörelerinin jeolojisi. MTA Report No. **6547** (in Turkish, Unpublished).

Akdeniz, N. and Konak, N. (1979b) Menderes masifinin Simav dolayındaki kaya birimleri ve metabazik, metaultramafik kayaların konumu. *Türkiye Jeoloji Kurumu Bülteni*, **22**, 175−183.

Balan, E., Saitta, A.M., Mauri, F., and Calas, G. (2001) First-principles modeling of the infrared spectrum of kaolinite. *American Mineralogist*, **86**, 1321−1330.

Balan, E., Lazzeri, M., Saitta, A.M., Allard, T., Fuchs, Y., and Mauri, F. (2005) First-principles study of OH-stretching modes in kaolinite, dickite, and nacrite. *American Mineralogist*, **90**, 50−60.

Benco, L., Tunega, D., Hafner, J., and Lischka, H. (2001) Orientation of OH groups in kaolinite and dickite: Ab initio molecular dynamics study. *American Mineralogist*, **86**, 1057−1065.

Bobos, I., Duplay, J., Rocha, J., and Gomes, C. (2001) Kaolinite to halloysite-7 Å transformation in the kaolin deposit of São Vicente de Pereira, Portugal. *Clays and Clay Minerals*, **49**, 596−607.

Braide, S.P. and Huff, W.D. (1986) Clay mineral variation in Tertiary sediments from the eastern Flank of the Niger Delta. *Clay Minerals*, **21**, 211−224.

Brindley, G.W. (1980) Quantitative X-ray analysis of clays. Pp. 411−438 in: *Crystal Structures of Clay Minerals and their X-ray Identification* (G.W. Brindley and G. Brown, editors). Monograph **5**, Mineralogical Society, London.

Burçak, M., Sevim, F., and Hacisalihoglu, O. (2007) Discovering a new buried geothermal field found using geological-geophysical and geochemical methods in Uchbash-Shaphane, Kutahya western Anatolia, Turkey. *Thirty-Second Workshop on Geothermal Reservoir Engineering, Proceedings, Stanford University*, *California*, SGP-TR-183, pp. 2−3.

Campbell, A.C., Palmer, M.R., Klinkhammer, G.P., Bowers, T.S., Edmond, J.M., Lawrence, J.R., Casey, J.F., Thompson, G., Humphris, S., Rona, P., and Karson, J.A. (1988) Chemistry of hot springs on the Mid-Atlantic ridge: TAG and MARK Sites. *Nature*, **335**, 514−519.

Churchman, G.J. and Gilkes, R.J. (1989) Recognition of intermediates in the possible transformation of halloysite to kaolinite in weathering profiles. *Clay Minerals*, **24**, 579−590.

Çiftçi, N.B. and Bozkurt, E. (2009) Evolution of the Miocene sedimentary fill of the Gediz Graben, SW Turkey. *Sedimentary Geology*, **216**, 49−79.

Clayton, R.N. and Mayeda, T.K. (1963) The use of bromine pentafluoride in the extraction of oxygen from oxides and silicates for isotopic analysis. *Geochimica et Cosmochimica Acta*, **27**, 43−52.

Çoban, F. (2001) Çayırlık Tepe perlitinin (Başören-Kütahya) bentonite alterasyonu sırasında majör, eser ve nadir toprak elementlerinin mobilizasyonu. *10th Ulusal Kil Sempozyumu*, 282−304.

Ece, I. and Yüce, A.E. (1999) *Endüstriyel mineraller envanteri, Yurt Madenciliğini Geli*ştirme Vakfı. Mart Matbaacılık Sanatları Ltd. Şti., pp. 77−83.

Erhenberg, S.N. (1991) Kaolinized, potassium-leached zones at the contacts of the Garn Formation, Haltenbanken, mid-Norwegian continental shelf. *Marine and Petroleum Geology*, **8**, 250−269.

Ercan, T., Dinçel, A., Metin, S., Türkecan, A., and Günay, A. (1978) Uşak yöresindeki Neojen havzalarının jeolojisi (Geology of the Neogene basins in Uşak region). *Bulletin of the Geological Society of Turkey*, **21**, 97–106.

Ercan, T., Günay, E., and Savaşçın, M.Y. (1981–1982) Simav ve çevresindeki Senozoyik yaşlı volkanizmanın bölgesel yorumlanması. *MTA Dergisi*, **97/98**, 86–101.

Farmer, V.C. (1974) The layer silicates. Pp. 331–364 in: *The Infrared Spectra of Minerals* (V.C. Farmer, editor). Monograph **4**, Mineralogical Society, London.

Faure, G. (1986) *Principles of Isotope Geology*, 2nd edition. John Wiley and Sons, New York, 589 pp.

Felhi, M., Tlili, A., Gaied, M.E., and Montacer, M. (2008) Mineralogical study of kaolinitic clays from Sidi El Bader in the far North of Tunisia. *Applied Clay Science*, **39**, 208–217.

Fulignati, P., Gioncada, A., and Sbrana, A. (1999) Rare earth element (REE) behaviour in alteration facies of the active magmatic–hydrothermal system of Vulcano (Aeolian Islands, Italy). *Journal of Volcanology and Geothermal Research*, **88**, 325–342.

Gilg, H.A., Weber, B., Kasbohm, J., and Frei, R. (2003) Isotope geochemistry and origin of illite-smectite and kaolinite from the Seilitz and Kemmlitź kaolin deposits, Saxony, Germany. *Clay Minerals*, **38**, 95–112.

Helvacı, C. (1984) Occurence of rare borate minerals: Veatchite–A, tunellite, teruggite and cahnite in the Emet borate deposits, Turkey. *Mineralium Deposita*, **19**, 217–226.

Huang, W.H. (1974) Stabilities of kaolinite and halloysite in relation to weathering of feldspar and nepheline in aqueous solution. *American Mineralogist*, **59**, 365–371.

Işık, İ., Uz, V., and Alver, Z. (2001) Çayca yöresi (Kütahya) tüflerinin karakterizasyonu ve seramik endüstrisinde kullanım olanakları. *10th Ulusal Kil Sempozyumu*, pp. 480–492.

Inoue, A. (1995) Formation of Clay Minerals in Hydrothermal Environments. Pp. 268–329 in: *Origin and Mineralogy of Clays* (B. Velde, editor). Springer-Verlag, Berlin.

Jepson, W.B. and Rowse, J.B. (1975) The composition of kaolinite; an electron microscope microprobe study. *Clays and Clay Minerals*, **23**, 310–317.

Johnston, C.T., Agnew, S.F., and Bish, D.L. (1990) Polarized single-crystal Fourier-transform infrared microscopy of Ouray dickite and Keokuk kaolinite. *Clays and Clay Minerals*, **38**, 573–583.

Kadir, S. and Karakaş, Z. (2002) Mineralogy, chemistry and origin of halloysite, kaolinite and smectite from Miocene ignimbrites, Konya, Turkey. *Neues Jahrbuch für Mineralogie, Abhandlungen*, **177**, 113–132.

Kadir, S. and Akbulut, A. (2009) Mineralogy, geochemistry and genesis of the Taşoluk kaolinite deposits in pre-Early Cambrian metamorphites and Neogene volcanites of Afyonkarahisar, Turkey. *Clay Minerals*, **44**, 89–112.

Kadir, S. and Kart, F. (2009) Occurrence and origin of the Söğüt kaolinite deposits in the Paleozoic Saricakaya granite-granodiorite complexes and overlying Neogene sediments (Bilecik, Northwestern Turkey). *Clays and Clay Minerals*, **57**, 311–329.

Karakaya, N. (2009) REE and HFS element behaviour in the alteration facies of the Erenler Dağı Volcanics (Konya, Turkey) and kaolinite occurrence. *Journal of Geochemical Exploration*, **101**, 185–208.

Konak, N. (2007) *1/500,000 scale geological map of Turkey – İzmir*. General Directorate of Mineral Research and Exploration of Turkey.

Kunze, G.W. and Dixon, J.B. (1986) Pretreatment for mineralogical analysis. Pp. 91–99 in: *Methods of Soil Analysis, Part I, Physical and Mineralogical Methods* (A. Klute, editor). Second edition, Madison, Wisconsin, USA.

Lavery, N.G. (1985) Quantifying chemical changes in hydrothermally altered volcanic sequences – silica enrichment as a guide to the Crandon massive sulfide deposit, Wisconsin, USA. *Journal of Geochemical Exploration*, **24**, 1–27.

MacKenzie, R.C. (1957) *The Differential Thermal Investigation of Clays*. Monograph **3**, Mineralogical Society, London, 456 pp.

MacLean, W.H. and Kranidiotis, P. (1987) Immobile elements as monitors of mass transfer in hydrothermal alteration: Phelps Dodge massive sulfide deposits, Matagami, Quebec. *Economic Geology*, **2**, 951–962.

Madejová, J., Kečk, K., Pálková, H., and Komadel, P. (2002) Identification of components in smectite/kaolinite mixtures. *Clay Minerals*, **37**, 377–388.

Meunier, A. (2005) *Clays*. Springer-Verlag, Berlin, Heidleberg, 472 pp.

Meunier, A. and Velde, B. (2004) *Illite: Origin, Evolution and Metamorphism*. Springer-Verlag, Berlin, Heidelberg, New York, 286 pp.

Mongelli, G. (1997) Ce-anomalies in the textural components of Upper Cretaceous karst bauxites from the Apulian carbonate platform (southern Italy). *Chemical Geology*, **140**, 69–79.

Moore, D.M. and Reynolds, R.C. (1989) *X-ray Diffraction and the Identification and Analysis of Clay Minerals*. Oxford University Press, New York, 332 pp.

Mutlu, H. and Güleç, N. (1998) Hydrogeochemical outline of thermal waters and geothermometry application in Anatolia (Turkey). *Journal of Volcanology and Geothermal Research*, **85**, 495–515.

Mutlu, H., Sarıiz, K., and Kadir, S. (2005) Geochemistry and origin of the Şaphane alunite deposit, Western Anatolia, Turkey. *Ore Geology Reviews*, **26**, 39–50.

Nesbitt, H.W. and Markovics, G. (1997) Weathering of granidioritic crust, long-term storage of elements in weathering profiles and petrogenesis of siliciclastic sediments. *Geochimica et Cosmochimica Acta*, **61**, 1653–1670.

Njoya, A., Nkoumbou, C., Grosbois, C., Njopwouo, D., Njoya, D., Courtin-Nomade, A., Yvon, J., and Martin, F. (2006) Genesis of Mayouom kaolin deposit (western Cameroon). *Applied Clay Science*, **32**, 125–140.

Okut, M., Demirhan, M., and Köse, Z. (1978) *Kütahya ili Emet – Simav ilçeleri kaolen zuhurları ve dolaylarının jeoloji raporu*. MTA Report No. 6309 (in Turkish, Unpublished).

Özcan, A., Göncüoğlu, M.C., Turan, N., Uysal, Ş., Şentürk, K., and Işık, A. (1988) Late Paleozoik evolution of the Kütahya-Bolkardağı belt. *METU Journal of Pure and Applied Sciences*, **21**, 211–220.

Parry, W.T., Ballantyne, J.M., and Jacobs, D.C. (1984) Geochemistry of hydrothermal sericite from Roosevelt Hot Springs and the Tintic and Santa Rita porphyry copper systems. *Economic Geology*, **79**, 72–86.

Paterson, E. and Swaffield, R. (1987) Thermal analysis. Pp. 99–132 in: *A Handbook of Determinative Methods in Clay Mineralogy* (M.J. Wilson, editor). Blackie and Sons Limited, Glasgow, UK, 308 pp.

Pissaridges, A., Stewart, J.W.B., and Rennie, D.A. (1968) Influence of cation saturation of phosphorous adsorption by selected clay minerals. *Canadian Journal of Soil Science*, **48**, 151–157.

Ringwood, A.E. (1990) Slab-mantle interactions: Petrogenesis of intraplate magmas and structure of the upper mantle. *Chemical Geology*, **82**, 187–207.

Roy, P.D. and Smykatz-Kloss, W. (2007) REE geochemistry of the recent playa sediments from the Thar Desert, India: An implication to playa sediment provenance. *Chemie der Erde*, **67**, 55–68.

Saikia, N.J., Bharali, D.J., Sengupta, P., Bordoloi, D.,

Goswamee, R.L., Saikia, P.C., and Borthakur, P.C. (2003) Characterization, beneficiation and utilization of a kaolinite clay from Assam, India. *Applied Clay Science*, **24**, 93–103.

Savaşcin, Y. (1978) Foça-Urla Neojen volkanitlerinin mineralojik jeokimyasal incelemesi ve kökensel yorumu. Doçentlik Tezi, Ege Üniversitesi, Yerbilimleri Fakültesi, 74 s.

Savin, S.M. and Epstein, S. (1970) The oxygen and hydrogen isotope geochemistry of clay minerals. *Geochimica et Cosmochimica Acta*, **34**, 25–42.

Savin, S.M. and Lee, M. (1988) Isotopic studies of phyllosilicates. Pp. 189–223 in: *Hydrous Phyllosilicates* (S.W. Bailey, editor). Reviews in Mineralogy, **19**, Mineralogical Society of America, Washington, D.C.

Sayın, Ş.A. (2007) Origin of kaolin deposits: evidence from the Hisarcık (Emet-Kütahya) deposits, western Turkey. *Turkish Journal of Earth Sciences*, **16**, 77–96.

Şener, M. and Gevrek, A.İ. (1986) Simav-Emet-Tavşanlı yörelerinin hidrotermal alterasyon zonları. *Jeoloji Mühendisliği Dergisi*, **28**, 43–49.

Seyitoğlu, G., Anderson, D., Nowel, G., and Scott, B.C. (1997) The evolution from Miocene potassic to Quaternary sodic magmatism in Western Turkey: implication for enrichment processes in the lithospheric mantle. *Journal of Volcanology and Geothermal Research*, **76**, 127–147.

Sheppard, S.M.F., Nielsen, R.L. and Taylor, H.P. (1969) Oxygen and hydrogen isotope ratios of clay minerals from porphry copper deposits. *Economic Geology*, **64**, 755–777.

Sheppard, S.M.F. (1986) Characterization and isotopic variations in natural waters. Pp. 165–184 in: *Stable Isotopes in High-Temperature Geological Processes* (J.W. Valley, H.P. Taylor, Jr., and J.R. O'Neil, editors). Reviews in Mineralogy, **16**, Mineralogical Society of America, Washington, D.C.

Sheppard, S.M.F. and Gilg, H.A. (1996) Stable isotope geochemisty of clay minerals; The story of sloppy, silky, lumpy and tough, Cairns-Smith (1971). *Clay Minerals*, **31**, 1–24.

Shikazono, N., Ogawa, Y., Utada, M., Ishiyama, D., Mizuta, T., Ishikawa, N., and Kubota, Y. (2008) Geochemical behavior of rare elements in hydrothermally altered rocks of the Kuroko mining area, Japan. *Journal of Geochemical Exploration*, **98**, 65–79.

State Planning Organization of Turkey (2001) 8th Five-Year Development Plan, Mining Special Expert Commission Report, Volume 1, Industrial Minerals Sub-Commission, Ceramic clays–Kaolin–Pyrophyllite–Wollastonite–Talc Group, Ankara, 224 pp. (http://ekutup.dpt.gov.tr/madencil/sanayiha/oik622.pdf)

Taylor, S.R. and McLennan, S.M. (1985) *The Continental Crust: Its Composition and Evolution.* Blackwell, Oxford, UK, 312 pp.

Türkmenoğlu, A.G. and Işık, N.Y. (2008) Mineralogy, chemistry and potential utilization of clays from coal deposits in the Kütahya province, Western Turkey. *Applied Clay Science*, **42**, 63–73.

Üstün, H. and Yetiş, C. (2007) Hisarcık (Emet-Kütahya) güneyinin Neojen stratigrafisi. *60. Türkiye Jeoloji Kurultayı Bildiri Özleri*, 460–462.

Van der Marel, H.W. and Beutelspacher, H. (1976) *Atlas of IR Spectroscopy of Clay Minerals and their Admixtures*. Elsevier, Amsterdam, 396 pp.

Wilson, M.J. (1987) X-ray powder diffraction methods. Pp. 26–98 in: *A Handbook of Determinative Methods in Clay Mineralogy* (M.J. Wilson, editor). Blackie & Sons Ltd, Glasgow, UK.

Winchester, J.A. and Floyd, P.A. (1977) Geochemical discrimination of different magma series and their differentiation products using immobile elements. *Chemical Geology*, **20**, 325–343.

Yeh, H.W. and Savin, S.M. (1977) Mechanism of burial metamorphism of argillaceous sediments: 3. O isotope evidence. *Bulletin of the Geological Society of America*, **88**, 1321–1330.

Yıldız, A. and Kuşçu, M. (2001) Başören (Kütahya) bentonit yataklarının mineralojisi ve teknolojik özellikleri. *10. Ulusal Kil Sempozyumu*, 269–281.

Ziegler, K. (2006) Clay minerals of the Permian Rotliegend Group in the North Sea and adjacent areas. *Clay Minerals*, **41**, 355–393.

(*Received 6 December 2010; revised 26 August 2011; Ms. 522; A.E. W. Huff*)